NASA REPORT CR72397

A THEORETICAL STUDY OF COMBUSTION AND QUENCHING OF SOLID PROPELLANT ROCKET MOTORS DURING DEPRESSURIZATION

by

Edward A. Fletcher and Tsuyoshi Hiroki

prepared for

NATIONAL AERONAUTICS AND SPACE ADMINISTRATION

January 15, 1968

CONTRACT NAS 3-6294

Technical Management
NASA Lewis Research Center
Cleveland, Ohio
H. Bankaitis

University of Minnesota
Mechanical Engineering Department
Minneapolis, Minnesota 55455

NASA REPORT CR72397

A THEORETICAL STUDY OF COMBUSTION AND QUENCHING OF SOLID PROPELLANT ROCKET MOTORS DURING DEPRESSURIZATION

by

Edward A. Fletcher and Tsuyoshi Hiroki

prepared for

NATIONAL AERONAUTICS AND SPACE ADMINISTRATION

January 15, 1968

CONTRACT NAS 3-6294

Technical Management
NASA Lewis Research Center
Cleveland, Ohio

H. Bankaitis

University of Minnesota
Mechanical Engineering Department
Minneapolis, Minnesota 55455

A THEORETICAL STUDY OF COMBUSTION AND QUENCHING OF SOLID PROPELLANT ROCKET MOTORS DURING DEPRESSURIZATION

SUMMARY

The conservation equations in the solid and gas phases are coupled with the chamber overall mass balance equation to produce a method of computing transient burning rates in solid propellant motors. This method is used to compute burning rates during rapid depressurizations achieved by suddenly enlarging the exhaust nozzle. A nondimensional parameter characterizing the depressurization rate, D_s, is used to correlate the results. During depressurizations, burning rates are smaller than the steady state values at the corresponding chamber pressures. A quench occurs when the depressurization parameter, D_s, exceeds some critical value D_{sc}. The quench limit of a propellant can be given as a single curve on the $D_s \sim P_2/P_1$ plane, where P_1 is the initial chamber pressure and P_2 is the steady operating pressure corresponding to the enlarged nozzle area. The results are in reasonable agreement with experiments. The effects of several variables on the quench limit are discussed. Ways of improving the present theory are suggested.

INTRODUCTION

It has been observed that a solid propellant rocket motor can be quenched by a rapid decrease of chamber pressure. Depressurization can be achieved by enlargement of the throat area or by opening a vent. If the depressurization rate is high enough, a quench will occur even though the steady state chamber pressure corresponding to the enlarged throat area is well above the low pressure limit of stable combustion.

The first systematic study of this phenomenon was reported by Ciepluch[1]. He burned propellant slabs in a chamber of relatively small free volume. He achieved rapid depressurization by suddenly venting the chamber. He observed that a quench will occur if the chamber pressure is reduced at a rate greater than some critical rate. The critical rate was approximately proportional to the initial chamber pressure. The critical time was, therefore, nearly independent of the initial chamber pressure. The critical time in one motor need not be the same as that in another having a different geometry (chamber free-volume, propellant surface area) even with the same propellant. Ciepluch also studied the effects of propellant composition on the critical time[2]. The critical time was decreased by an increase in aluminum or ammonium perchlorate concentration. There was no correlation between the critical time and the strand burning rate.

One criterion for quenching might be that the burning rate goes to zero. A knowledge of the burning rate during pressure transients is, therefore,

essential. Transient ballistic performance has sometimes been evaluated with steady state burning rates[3]. Von Elbe[4] developed a theoretical model to predict nonsteady burning rates. He assumed that departures from steady state rates resulted from the slow readjustment of the temperature field in the solid. The relaxation time in the gas was assumed to be negligible. He treated a case of a moderate rate of pressure change. He assumed:

(A) The temperature profile in the solid is the same as that of the steady state at the corresponding burning rate.

(B) The heat flux from the gas phase is the same as the steady state value at the corresponding burning rate.

Von Elbe's rate law says that the burning rate at any instant is determined by the instantaneous chamber pressure and its time derivative. It also says that burning rates during depressurizations are smaller than steady state burning rates at the corresponding pressures. Thus, a quench might occur at some critical depressurization rate. He derived his equations by considering the behavior of the temperature readjustment process. The same thing can be done more concisely as follows: the integral form of the energy equation in the solid is,

$$c\bar{G}(\bar{T}_w - \bar{T}_i) = f_s - dq/dt \; * \qquad \text{(i)}$$

where f_s is the heat flux to the grain just inside the propellant surface** and q is the energy content in the solid. In the steady state $dq/dt = 0$, hence,

$$\bar{G}_{steady} = \frac{f_{s,\,steady}}{c(\bar{T}_w - \bar{T}_i)} \qquad \text{(ii)}$$

The term dq/dt must be positive in a depressurization process if combustion is to continue. Hence, if $f_{s,\,transient}$ is assumed to be equal to $f_{s,\,steady}$, equation (i) requires that the burning rate during depressurization be smaller than the steady state rate. When dp/dt has to be considered, the temperature gradient on the gas side of the surface must be larger to satisfy the energy balance at the surface. Then f_s in the depressurization must be larger than the steady state value. The applicability of assumption (A) to a rapid depressurization process may also be questionable. The same burning rate law, with a different constant was derived elsewhere[5].

---

* Von Elbe's basic equation has an error. It has the term 2dq/dt instead of dq/dt in equation (i).

** f_s is not the same as the heat flux from the gas phase f_g. They are related by $f_g - f_s = \Delta\bar{h}_w\bar{G}$. Von Elbe overlooked this difference.

In previous work[6] we described an experiment in which chamber gas was suddenly expanded into a secondary evacuated chamber. After a rapid depressurization as the secondary chamber was being filled, the pressure continued to decrease at a slower rate. The burning rate after depressurization was thus lower than the steady state rate at the same pressure.

A nonsteady burning rate theory has been proposed in connection with oscillating combustion.[7] A modification[8] permits inclusion of heterogeneous surface reactions. The nonsteady conservation equations were linearized around the steady state conditions by a small perturbation method. The first order response of burning rates to pressure transients was used to determine quenching criteria. A close relationship between quenching criteria and stability criteria was suggested. However, since the small perturbation method was used in the mathematical treatment, application of this theory to quenching may not be justified. The models of neither reference 4 nor 8 couple the overall gasdynamics (energy and mass conservation in the whole chamber) to the response of the solid to pressure disturbances. Hence, they do not give the effects of motor configuration on the quenching behavior.

It has also been observed[9] that combustion cannot be maintained at pressures below a critical pressure which depends on the characteristic length of the chamber. This is called L*-extinguishment in contrast to dp/dt-extinguishment. A propellant which is susceptible to L*-extinguishment is also susceptible to dp/dt-extinguishment[10]. This is interpreted[11] to mean that L*-extinguishment occurs because $d\bar{P}/d\bar{t}$ is amplified during the decreasing pressure phase of an oscillation. The measured $d\bar{P}/d\bar{t}$ at the point of L*-extinguishment is said to roughly correspond to $d\bar{P}/d\bar{t}$ at dp/dt-extinguishment.

Procedures for combustion termination by nozzle area variation have considered both mechanisms[12]. It was implicitly assumed that the critical time to produce a dp/dt-extinguishment is the same for all motors. This assumption has drawbacks. If depressurization is initiated by sudden opening of a secondary nozzle, the size of the secondary nozzle and the chamber volume determine the depressurization rate. If $\bar{P}_1$ is the initial chamber pressure and $\bar{P}_2$ the operating pressure when the motor uses both nozzles, the motor cannot be extinguished if $\bar{P}_2/\bar{P}_1$ is nearly one, no matter how large $d\bar{P}/d\bar{t}$ may be made by reducing the chamber volume or the propellant surface area. On the other hand when $\bar{P}_2/\bar{P}_1$ is nearly zero, the motor will be extinguished even when $d\bar{P}/d\bar{t}$ is small. The quench limit must, therefore, be determined by coupling chamber ballistics with a nonsteady burning rate law.

When a solid propellant motor is depressurized at non-zero ambient pressure, one of three things may occur: a quench, a burn-out or a reignition[13] in which the motor appears to have quenched for several seconds. Inert gas injection has virtually no effect on the occurrence of reignitions[14].

Solid phase reactions may play an important role in the process, however.

The present state of art in this field suggests that a sound theoretical framework is needed to provide a method for interpretation and correlation of the experimental data and to suggest meaningful experiments. Even though few kinetic or transport properties are known, such a framework can serve this purpose. The work described in this report is intended to do this. A method for computing transient burning rates is described. It is not restricted to small perturbations. For computational simplicity, the assumption is made that the adiabatic flame temperature remains constant during the pressure transient. The results, therefore, predict a need for higher depressurization rates to produce a quench than would be required if a more realistic temperature were used. The method can easily be modified to handle different flame temperatures. This method is then used to compute burning rates during rapid depressurization to obtain quenching limits in terms of appropriate parameters. The effects of motor configurations are included by coupling the chamber mass balance to the conservation equations in the solid and gas phases. The results are compared with experimental data. They are used to suggest natural parameters which should be used to correlate experiments and to suggest additional experiments and theoretical studies.

FORMALIZATION OF THE PROBLEM

In this section, a nonsteady one dimensional combustion model is presented. Since the flame is very thin compared with typical motor dimensions, a one dimensional model is probably a good approximation. The conservation equations in the solid and the gas phase are used. With the boundary conditions imposed at the propellant surface, the burning rate is determined uniquely as a "connecting coefficient" of these partial differential equations.

The problem is admittedly oversimplified. Thermodynamic and transport properties are assumed constant. A single step reaction of the order n, which may have fractional values, is assumed. Molecular weights of reactant and product are assumed to be equal.

Gas Phase

The continuity equation is,

$$\frac{\partial \bar{\rho}}{\partial \bar{t}} + \frac{\partial \bar{G}}{\partial \bar{x}} = 0 . \qquad (1)$$

If all diffusion coefficients are assumed equal and thermal diffusion is negligible, the conservation equation for species i is,

$$\frac{\partial \bar{\rho}_i}{\partial \bar{t}} + \frac{\partial \bar{G}_i}{\partial \bar{x}} = W_i(\bar{\rho}_i, \bar{T}) \tag{2}$$

where

$$\bar{\rho}_i = m_i \bar{\rho}$$

and

$$\bar{G}_i = m_i \bar{G} - \bar{\rho} D \frac{\partial m_i}{\partial \bar{x}} \quad .$$

We consider only species "reactant" and "product". Combination of equations (1) and (2) yields,

$$\bar{\rho} \frac{\partial m_1}{\partial \bar{t}} + \bar{G} \frac{\partial m_1}{\partial \bar{x}} - \bar{\rho} D \frac{\partial^2 m_1}{\partial \bar{x}^2} = W_1(\bar{\rho}_1, \bar{T}) \tag{3}$$

where the subscript 1 denotes reactant. The mass rate of formation of the reactant is given by,

$$W_1 = -K \bar{\rho}_1^{\,n} \exp(-\bar{E}/\bar{T}) \; . \tag{4}$$

The diffusion-thermo effect and kinetic energy of the gas are assumed negligible. If heat capacities of reactant and product are the same, the energy equation is,

$$\frac{\partial \bar{\rho}\, \bar{e}}{\partial \bar{t}} + \sum_i \frac{\partial \bar{G}_i \bar{h}_i}{\partial \bar{x}} = k_g \frac{\partial^2 \bar{T}}{\partial \bar{x}^2} \tag{5}$$

where

$$\bar{h}_i = c_p \bar{T} + \bar{h}^o_i \quad ,$$

$$\bar{h} = \sum_i m_i \bar{h}_i \quad ,$$

and

$$\sum_i \bar{G}_i \bar{h}_i = \bar{G} \sum_i m_i \bar{h}_i - \bar{\rho} D \sum_i \frac{\partial m_i}{\partial \bar{x}} \bar{h}_i$$

$$= \bar{G} \bar{h} - \bar{\rho} D \frac{\partial m_1}{\partial \bar{x}} (\bar{h}^o_1 - \bar{h}^o_2) \; .$$

The heat of chemical reaction at constant pressure is $\Delta \bar{h}^o = \bar{h}^o_1 - \bar{h}^o_2$. Combination of equation (5) with equations (1) and (2) yields,

$$\bar{\rho}\, c_p \frac{\partial \bar{T}}{\partial \bar{t}} + \bar{G} c_p \frac{\partial \bar{T}}{\partial \bar{x}} - \frac{\partial \bar{P}}{\partial \bar{t}} - k_g \frac{\partial^2 \bar{T}}{\partial \bar{x}^2} = - \Delta \bar{h}^o W_1 \quad . \tag{6}$$

Multiplying equation (3) by $\Delta \bar{h}^o$ and adding the result to equation (6), one obtains,

$$\bar{\rho} \frac{\partial \bar{h}}{\partial \bar{t}} - \frac{\partial \bar{P}}{\partial \bar{t}} + \bar{G} \frac{\partial \bar{h}}{\partial \bar{x}} - \frac{k}{c_p} \frac{\partial^2 \bar{h}}{\partial \bar{x}^2} - \frac{k}{c_p} (L_e - 1) \Delta \bar{h}^o \frac{\partial^2 m_1}{\partial \bar{x}^2} = 0 \quad . \tag{7}$$

It is now assumed that the Lewis number is one. Then $k/c_p = \rho D = \Gamma_g$ and equation (7) becomes,

$$\bar{\rho} \frac{\partial \bar{h}}{\partial \bar{t}} - \frac{\partial \bar{P}}{\partial \bar{t}} + \bar{G} \frac{\partial \bar{h}}{\partial \bar{x}} - \Gamma_g \frac{\partial^2 \bar{h}}{\partial \bar{x}^2} = 0 \quad . \tag{8}$$

We remove the momentum equation by assuming that the pressure in the combustion zone is uniform, i.e., $P = P(\bar{t})$. When the throat area is suddenly enlarged, the pressure in the combustion zone starts to change when the rarefaction wave first reaches it. By this time the rarefaction wave is much thicker than the flame even though the rarefaction may have started as a centered wave. Pressure gradients in the combustion zone can, therefore, be neglected.

The boundary conditions at the propellant surface are: continuity of mass flux,

$$\bar{G}_s(\bar{t}) = \bar{G}_g(0, \bar{t}) \quad , \tag{9}$$

continuity of temperature,

$$\bar{T}_s(0, \bar{t}) = \bar{T}_g(0, \bar{t}) = \bar{T}_w \quad , \tag{10}$$

continuity of species mass flux,

$$\bar{G}_s(\bar{t}) = \bar{G}_g(0, \bar{t})\, m_1 - \bar{\rho} D \left(\frac{\partial m_1}{\partial \bar{x}} \right)_w \quad , \tag{11}$$

and energy balance,

$$k_s \left(\frac{\partial \bar{T}}{\partial \bar{x}} \right)_{s,w} = k_g \left(\frac{\partial \bar{T}}{\partial \bar{x}} \right)_{g,w} - \Delta \bar{h}_w \bar{G}_s(\bar{t}) \quad . \tag{12}$$

Combination of equations (11) and (12) gives the boundary condition for equation (8),

$$(\Delta\bar{h}^{o} + c_p\bar{T}_w - \Delta\bar{h}_w)\,\bar{G}_s - k_s\left(\frac{\partial\bar{T}}{\partial\bar{x}}\right)_{s,w} = \bar{G}_s\bar{h}_w - \left(\Gamma_g\frac{\partial\bar{h}}{\partial\bar{x}}\right)_{g,w}\ , \qquad (13)$$

where $\Delta\bar{h}_w$ is the enthalpy change of the surface reaction. It is positive for endothermic reactions.

The surface temperature is assumed to remain constant during depressurization. Since the surface reaction is a rate process, a rate equation of the form,

$$\bar{G}_s(\bar{t}) = B\exp(-\bar{E}_w/\bar{T}_w) \qquad (*)$$

may be a better one. However, studies of the pyrolysis rates of propellant components suggest that E_w is large. Thus, for a wide variation of burning rates, the surface temperature should stay almost constant. Measurements of surface temperatures at various operating pressures[16] support this contention.

The initial temperature and concentration profiles are given by solutions of the steady state equations; the initial mass flow rate profiles are not. If the pressure in the chamber is uniform, the continuity equation applied to the whole chamber gives a pressure versus time relation of the type $\bar{P} = \bar{P}_1(-c\bar{t})$ near $\bar{t} = 0$. If $d\bar{P}/d\bar{t}$ (hence, $d\bar{\rho}/d\bar{t}$) is not zero at $\bar{t} = 0$, equation (1) requires that $d\bar{G}/d\bar{x}$ be non-zero at $\bar{t} = 0$, although $\bar{G}$ is constant along $\bar{x}$ before depressurization. This results from our neglect of the momentum equation, i.e., the acceleration time is assumed negligibly small. The gas velocity undergoes an almost discontinuous change but the position of each gas element does not change. Consequently, the temperature and the concentration profiles stay unchanged. Initial values of $\bar{T}$ and m_i can be given by the solution of the steady state equations, initial values of $\bar{G}$ by the solution of equation (1) with the initial value of $d\bar{P}/d\bar{t}$.

Solid Phase

It is assumed that there is no chemical reaction in the solid.

If a coordinate system fixed with respect to the propellant surface is used, the energy equation is,

$$\rho_s c\,\frac{\partial\bar{T}}{\partial\bar{t}} + c\bar{G}(\bar{t})\,\frac{\partial\bar{T}}{\partial\bar{x}} = k\,\frac{\partial^2\bar{T}}{\partial\bar{x}^2} \qquad (14)$$

The boundary condition is, $\quad T(0,\bar{t}) = \bar{T}_w$.

If the coordinate system fixed with respect to the solid is used, the energy equation becomes,

$$\rho_s c \frac{\partial \bar{T}}{\partial \bar{t}} = \frac{\partial^2 \bar{T}}{\partial \bar{x}^2} \tag{15}$$

with the boundary condition

$$\bar{T} = \bar{T}_w \qquad \text{at} \quad \bar{x} = -\int_0^{\bar{t}} \frac{\bar{G}}{\rho}\, d\bar{t} \ .$$

For both coordinate systems the initial data are given by the solution of,

$$\bar{G} \frac{d\bar{T}}{dy} = \frac{k}{c} \frac{d^2\bar{T}}{dy^2} \ , \qquad y = \bar{x}' = \bar{x} \ , \tag{16}$$

with the boundary conditions,

$$\bar{T}\,(0, \bar{t}) = \bar{T}_w$$

and

$$\bar{T}\,(-\infty, \bar{t}) = \bar{T}_i \ .$$

The equation for energy balance at the propellant surface is used with these equations.

If $\bar{P}$ and $\bar{G}$ are prescribed and the boundary condition (12) is removed, the solid and gas phase equations can be solved separately. The burning rate $\bar{G}_s$ is the "connecting coefficient" which must be determined to satisfy equation (12).

Chamber Gas Dynamics

Equations (1) to (16) can be used to compute burning rates if $P\,(\bar{t})$ is prescribed. However, since depressurizations are usually achieved by alteration of the engine hardware, $P\,(\bar{t})$ is an unknown variable to be determined. The quench limit is determined only when chamber gas dynamics is combined with a propellant burning rate law. In this study depressurization is assumed to be achieved by a sudden opening of a vent nozzle.

When the ambient pressure is zero, the mass conservation equation is,

$$V_c \frac{d\bar{\rho}}{d\bar{t}} = \bar{G}_s A_p - (\dot{m}_t + \dot{m}_v) \ . \tag{17}$$

Pressure and temperature are assumed to be uniform in the chamber. If the nozzle throats are choked immediately, the mass flow through the nozzle

is given by,

$$\dot{m}_t + \dot{m}_v = C_1(A_t + A_v)\frac{\bar{P}}{\sqrt{\bar{T}}} \tag{18}$$

where

$$C_1 = \left(\frac{2}{\gamma+1}\right)^{\frac{1}{\gamma+1}}\sqrt{\frac{2\gamma}{(\gamma+1)R}}\ .$$

The $\bar{P}\sim\bar{T}$ relationship has a minor effect on $\bar{P}\sim\bar{G}$ relationship[6]. For simplicity we assume an isothermal process here. If $\bar{P}_1$ and $\bar{P}_2$ are the steady state chamber pressures corresponding to the throat areas A_t and $(A_t + A_v)$ and steady burning follows Viellie's law,

$$\left(\frac{\bar{P}_2}{\bar{P}_1}\right)^{(1-m)} = \frac{A_t}{A_t + A_v} \tag{19}$$

Combination of equations (17), (18) and (19) yields,

$$\frac{1}{C_1}\left(\frac{\bar{P}_2}{\bar{P}_1}\right)^{(1-m)}\frac{V_c}{A_t R\bar{P}_1\bar{T}_f^{1/2}}\frac{d\bar{P}}{dt} = \left(\frac{\bar{P}_2}{\bar{P}_1}\right)^{(1-m)}\frac{\bar{G}}{\bar{G}_1} - \frac{\bar{P}}{\bar{P}_1}\ , \tag{20}$$

where $\bar{G}_1$ is the steady state burning rate at $\bar{P}_1$.

When the ambient pressure is not zero, the depressurization process is the same until the chamber pressure reaches the critical pressure. After this the mass flow rate through the nozzles is,

$$\dot{m}_t + \dot{m}_v = \sqrt{\frac{2\gamma}{R(\gamma-1)}}\frac{\bar{P}}{\bar{T}_f^{1/2}}(A_{te} + A_{ve})\sqrt{\left(\frac{\bar{P}_a}{\bar{P}}\right)^{2/\gamma} - \left(\frac{\bar{P}_a}{\bar{P}}\right)^{(\gamma+1)/\gamma}}\ . \tag{21}$$

Equation (17) becomes

$$\frac{1}{C_1}\left(\frac{\bar{P}_2}{\bar{P}_1}\right)^{(1-m)}\frac{V_c}{A_t R\bar{P}_1\bar{T}_f^{1/2}}\frac{d\bar{P}}{dt} = \left(\frac{\bar{P}_2}{\bar{P}_1}\right)^{(1-m)}\frac{\bar{G}}{\bar{G}_1} - \frac{\bar{P}}{\bar{P}_1}\frac{A_{te}+A_{ve}}{A_t+A_v} \times$$

$$\sqrt{\frac{\gamma+1}{\gamma-1}}\left(\frac{\gamma+1}{2}\right)^{1/(\gamma-1)}\sqrt{\left(\frac{\bar{P}_a}{\bar{P}}\right)^{2/\gamma} - \left(\frac{\bar{P}_a}{\bar{P}}\right)^{(\gamma+1)/\gamma}} \tag{22}$$

where A_{te} and A_{ve} are the nozzle exit areas, and $\bar{P}_1$ and $\bar{P}_2$ are assumed to be above the critical pressure. The critical pressure ratio is given by,

$$\left(\frac{\bar{P}_a}{\bar{P}}\right)_{crit.} = \left(\frac{2}{\gamma+1}\right)^{\gamma/(\gamma-1)} \tag{23}$$

Non-Dimensionalization

We define the following non-dimensional variables: $x = \bar{x}/\overset{*}{x}$, $t = \bar{t}/\overset{*}{t}$, $h = \bar{h}/\overset{*}{h}$, $P = \bar{P}/\overset{*}{P}$, $T = \bar{T}/\overset{*}{T}$, $E = \bar{E}/\overset{*}{E}$ and $G = \bar{G}/\overset{*}{G}$. The non-dimensionalizing quantities $\overset{*}{x}$, $\overset{*}{t}$, etc, should be chosen in such a way that the magnitudes of such factors as $\partial T/\partial x$, etc, in the equations are of the order one; the magnitudes of the terms themselves are now determined only by the magnitudes of the non-dimensional parameters. At the same time the number of non-dimensional parameters should be minimized. The obvious choices are,

$$\overset{*}{P} = \bar{P}_1,\ \overset{*}{T} = \bar{T}_w,\ \overset{*}{G} = \bar{G}_1,\ \overset{*}{E} = \overset{*}{T}_w,\ \overset{*}{h} = c_p \bar{T}_w \quad .$$

The choices for $\overset{*}{T}$ and $\overset{*}{E}$ are somewhat arbitrary. We will choose $\overset{*}{t}$ in such a way that the non-dimensional depressurization rate dP/dt is -1 at $t = 0$. Thus, $\overset{*}{t}$ is the characteristic time of depressurization. From equation (18),

$$\overset{*}{t} = V_c/(C_1 A_t R \bar{T}_f^{1/2})\,(\bar{P}_2/\bar{P}_1)^{1-m}/(1 - (\bar{P}_2/\bar{P}_1)^{1-m}) \quad . \tag{24}$$

We define different $\overset{*}{x}$'s in the solid and gas phases because the thicknesses of the thermal layers in the two phases are different. The steady state energy equation suggests the following definitions:

$$\overset{*}{x}_s = \Gamma_s/\bar{G}_1 \qquad \text{in the solid phase,}$$

and

$$\overset{*}{x}_g = \Gamma_g/\bar{G}_1 \qquad \text{in the gas phase.}$$

The resultant non-dimensional equations can now be written.

Gas phase. The continuity equation (1) becomes,

$$D_g \frac{\gamma}{\gamma - 1} \frac{\partial}{\partial t}\left(\frac{P}{T}\right) + \frac{\partial G}{\partial x} = 0 \tag{25}$$

where

$$D_g = \frac{\bar{P}_1 \Gamma_g}{\overset{*}{t}\, c_p \bar{T}_w \bar{G}_1^2} \quad .$$

The energy equation (6) becomes,

$$D_g\left(\frac{\gamma}{\gamma-1}\ \frac{P}{T}\ \frac{\partial T}{\partial t} - \frac{\partial P}{\partial t}\right) + G\frac{\partial T}{\partial x} - \frac{\partial^2 T}{\partial x^2} = A\left(\frac{P}{T}\right)^n m_1^n \exp(-E/T) \tag{26}$$

where

$$A = \frac{K\,\Delta\bar{h}^o \bar{P}_1^n \sqrt{\ }}{c_p \bar{T}_w^{n+1} R^n \bar{G}_1^2} .$$

Equation (8) becomes,

$$D_g\left(\frac{\gamma}{\gamma-1}\ \frac{P}{T}\ \frac{\partial h}{\partial t} - \frac{\partial P}{\partial t}\right) + G\frac{\partial h}{\partial x} - \frac{\partial^2 h}{\partial x^2} = 0 . \tag{27}$$

The boundary conditions are:

$$G_s(t) = G_g(0,t), \tag{28}$$

$$T_s(0,t) = T_g(0,t) = 1, \tag{29}$$

$$\frac{c}{c_p}\ \frac{\partial T}{\partial x}\Big)_{s,w} = \frac{\partial T}{\partial x}\Big)_{g,w} - \Delta h_w G_s(t), \tag{30}$$

and

$$(\Delta h^o - \Delta h_w + 1)\, G_s - \frac{c}{c_p}\ \frac{\partial T}{\partial x}\Big)_{s,w} + \frac{\partial h}{\partial x}\Big)_{g,w} = G_s h_{g,w} . \tag{31}$$

The initial values of T and h are given by the solution of,

$$\frac{dT}{dx} - \frac{d^2 T}{dx^2} = A\left(\frac{P}{T}\right)^n m_1^n \exp(-E/T) = 0 \tag{32}$$

and

$$\frac{dh}{dx} - \frac{d^2 h}{dx^2} = 0 . \tag{33}$$

Elimination of $\partial T/\partial t$ from equations (25) and (26) and substitution into equation (32) gives initial values of G.

$$G(x,0) = 1 - D_g \frac{1}{\gamma-1}\ \frac{dP}{dt}\ x . \tag{34}$$

Solid phase. Equation (13) becomes,

$$D_s \frac{\partial T}{\partial t} + G \frac{\partial T}{\partial x'} = \frac{\partial^2 T}{\partial x'^2} \tag{35}$$

where

$$D_s = \frac{\rho_s \kappa_s}{{}^*_t G_1^2}$$

with the boundary condition,

$$T(0,t) = 1 . \tag{35'}$$

Equation (14) becomes,

$$D_s \frac{\partial T}{\partial t} = \frac{\partial^2 T}{\partial x^2} \tag{36}$$

with the boundary condition,

$$T = 1 \qquad \text{at} \qquad s = -\int_o^t \frac{G}{D_s}\, dt . \tag{36'}$$

The steady state equation (20) becomes,

$$\frac{dT}{dy} = \frac{d^2 T}{dy^2} \tag{37}$$

with the boundary conditions,

$$T(0) = 1$$

and

$$T(-\infty) = T_i .$$

Chamber gas dynamics. The ballistic equation (20) becomes

$$\left(1/\left[1-(P_2/P_1)^{1-m}\right]\right) \frac{dP}{dt} = (P_2/P_1)^{1-m} G - P . \tag{38}$$

The ballistic equation for subcritical pressures (22) becomes,

$$\frac{1}{1-\left(\frac{P_2}{P_i}\right)^{(1-m)}} \frac{dP}{dt} = \left(\frac{P_2}{P_1}\right)^{(1-m)} G - P \frac{A_{te} + A_{ve}}{A_t + A_v} \sqrt{\frac{\gamma+1}{\gamma-1}} \left(\frac{\gamma+1}{2}\right)^{1/(\gamma-1)} \sqrt{\left(\frac{P_a}{P}\right)^{\frac{2}{\gamma}} - \left(\frac{P_a}{P}\right)^{\frac{\gamma+1}{\gamma}}} . \tag{39}$$

If the burning rate differs from the steady state rate during a transient, the difference comes from the time dependent terms in the governing equations. All time dependent terms are associated with D_s and D_g; these parameters, therefore, determine the magnitude of departure. D_s and D_g represent the ratios of the temperature response times in the solid and gas phases to the characteristic time for depressurization.

Evaluation of Non-Dimensional Parameters

To evaluate the non-dimensional parameters and carry out numerical calculations, we need thermodynamic properties, transport properties, and chemical kinetic data.

It will be shown later that the present theory gives the relationship between the gas phase reaction order and pressure exponent of the steady state burning rate as $n = 2m$. Knowledge of the preexponential coefficient is not needed if the steady state burning rate at any chamber pressure is known. Physical and chemical properties of typical composite propellants are listed in Table 1. The values in the third column were used in numerical calculations.

TABLE 1

VALUES OF PHYSICAL QUANTITIES USED IN COMPUTATIONS

	typical values	values used in calculations
m	0.3 – 0.8	0.4, 0.5, 0.6
$\bar{E}(E)$	5000 – 15000°K	5000°K(5.56), 10000°K(11.12)
$\Delta\bar{h}_w(h_w)$	± 100 cal/g[16]	-90 cal/g(-0.2), 0, +90 cal/g
c	0.28 – 0.3 cal/g°K[17]	0.3 cal/g°K
c_p	0.45 – 0.67 cal/g°K	0.5 cal/g°K
k_s	9.8×10^{-4} cal/°C sec. cm[17]	
k_g	2.0×10^{-4} cal/°C sec. cm	
$\bar{T}_w(T_w)$	800 – 1000°K[16]	900°K
$\bar{T}_f(T_f)$	2500 – 3500°K	2700°K
$\bar{T}_i(T_i)$	300°K	300°K
$\bar{\rho}_s$	1.7 g/cm^3	

Three values of m, two values of E and three values of Δh_w were selected for the computations. In this way the effects of variations in propellant properties were observed. All other values were fixed. The cases of endothermic, neutral and exothermic surface reactions having enthalpy changes of +90 cal/g, 0, -90 cal/g corresponding to $\Delta h_w = 0.2$, 0, and -0.2 are considered, since they represent a range of possible values[16].

D_s and D_g represent the temperature relaxation times in the solid and gas phases. A small value of D_s or D_g corresponds to a quick response to a pressure disturbance. If we use the property values listed in Table 1, they become,

$$D_s = \frac{\rho_s \int_s}{\bar{G}_1^2 \overset{*}{t}} = 55.4\times10^{-4}\, 1/\bar{G}_1 \overset{*}{t} \qquad (\bar{G}_1 \text{ in g/sec.cm}^2, \overset{*}{t} \text{ in sec})$$

and

$$D_g = \frac{\int_g}{c_p \bar{T}_w \bar{G}_1^2} \frac{\bar{P}_1}{\overset{*}{t}} = 1.465\, \bar{P}_1/\overset{*}{t} \qquad (\bar{P}_1 \text{ in psia}) \ .$$

A typical ammonium perchlorate composite propellant quenches when $\overset{*}{t} = 0.67\times10^{-2}$ sec. or $d\bar{P}/d\bar{t} = 0.7\times10^{5}$ psi/sec. at 500 psia. At the quench limit, then, $D_s = 0.827$ and $D_g = 1.025\times10^{-4}$. We have chosen the non-dimensionalizing quantities so that all the derivatives and the reaction terms are of the order of one in our non-dimensionalized equations. It may, therefore, be concluded that, if $d\bar{P}/d\bar{t}$ is not extremely large, in the gas phase the time dependent terms are negligibly small. This means that the relaxation time in the gas is very short.

We may tentatively summarize our consideration of the problem as follows. When $\bar{P}_1 \simeq 500$psia, $\bar{G}_1 \simeq 1$ g/cm^2 sec., and if $d\bar{P}/d\bar{t} < 10^3$ psi/sec., the whole process is quasi-steady and the burning rate follows the steady state law. If 10^4 psi/sec $< d\bar{P}/d\bar{t} < 10^7$ psi/sec, relaxation time in the gas phase is still negligible but it cannot be neglected in the solid phase. If $d\bar{P}/d\bar{t} > 10^8$ psi/sec., relaxation times are not negligible in either phase. Since we are interested in the range $d\bar{P}/d\bar{t} = 10^4 \sim 10^6$ psi/sec., our mathematical problem is greatly simplified.

Final Formulation

When x is large and G is small, terms containing D_g may not be neglected. Far from the propellant surface, all other terms in the energy equation become comparable with D_g. Very far from the surface, the nonsteady term predominates. The energy equation (26) reduces to,

$$\frac{\gamma}{\gamma-1} \frac{P}{\bar{T}} \frac{\partial T}{\partial t} - \frac{\partial P}{\partial t} = 0 \ .$$

The solution of this equation is

$$T^{\gamma}/P^{\gamma-1} = \text{const.}$$

Thus, outside the flame zone, the $P \sim T$ relationship is isentropic for all depressurization rates. If depressurization is very slow, the chamber temperature does not change; a succession of the steady states is observed. This apparent contradiction is explained as follows: The flame zone (zone of non-uniform temperature) is different in steady and nonsteady states. Consider a gas element which just emerges from the propellant surface as depressurization starts. The temperature of this element increases because of its own combustion and conduction. Some of the temperature increase is sacrificed by the expansion work due to the depressurization. However, the chemical reaction zone is so thin that the pressure has decreased very little by the time the element has been completely burned. The temperature of this element is almost adiabatic flame temperature. The temperature of the element then decreases as it expands. In a real motor when the pressure change is slow, the gas element has left the exhaust nozzle before the temperature or pressure decreases appreciably. Even if depressurization is fast, the temperature at the end of the reaction zone is almost adiabatic flame temperature. For the purposes of this computation , transient additional heat losses to the solid are ignored although they are undoubtedly significant.

Terms associated with D_g also become comparable to the other terms near the end of the depressurization process when the burning rate becomes very small. By this time, however, the important features of the process have been determined. The relative magnitudes of D_s and D_g do not change. We therefore neglect all D_g terms and assume that the temperature at the end of the reaction zone is the adiabatic flame temperature. The steady state equations (32) and (33) are then valid for nonsteady states as well. From equation (34) we obtain,

$$\Delta G/G \simeq 1 + D_g$$

where ΔG is an increase in G due to acceleration of the gas. We may, therefore assume that G is a function of time only and equation (25) can be removed.

Now it is more convenient to use a new space coordinate defined by,

$$\eta_g = \frac{\bar{x}\bar{G}(t)}{\Gamma_g} \qquad \text{in the gas phase}$$

and

$$\eta_s = \frac{\bar{x}\bar{G}(t)}{\Gamma_s} \qquad \text{in the solid phase.}$$

Equations (32) and (33) can now be written

$$\frac{d^2T}{d\eta^2} - \frac{dT}{d\eta} + A'\left(\frac{P}{T}\right)^n m_1^n \exp(-E/T) = 0 \qquad (40)$$

where

$$A' = A/G^2$$

and

$$\frac{d^2h}{d\eta^2} - \frac{dh}{d\eta} = 0 \quad . \qquad (41)$$

Boundary conditions for (40) and (41) are given by equations (28) through (31). In the solid phase, D_s is of the order one; hence the energy equation (35) or (36) remains the same.

SOLUTION

Gas Phase Equations

In the gas phase equations (32) and (33) can be used at each instantaneous time. However, because the boundary conditions at the surface are time dependent, the solution is different from that of the steady state.

The general solution of equation (41) is given by,

$$h = C_1 + C_2 e^{\eta} \quad .$$

Since $h < \infty$ at $\eta = \infty$,

$$h = C_1 \quad .$$

No reverse reaction is considered; $m_1 = 0$ at $\eta = \infty$, and

$$C_1 = h_\infty = T_\infty + m_{1\infty} h^o = T_f \quad .$$

Hense,

$$m_1 = \frac{T_f - T}{\Delta h^o} \qquad (42)$$

Substitution into equation (40) yields,

$$\frac{d^2T}{d\eta^2} - \frac{dT}{d\eta} + \frac{1}{\lambda^2}\left(\frac{T_f}{T} - 1\right)^n \exp(-E/T) = 0 \qquad (43)$$

where

$$\lambda = \frac{G}{P^{n/2}} \left(\frac{\bar{G}_1^2 \bar{T}_w R^n \Delta \bar{h}^{o(n-1)}}{\bar{P}_1^n K \Gamma_g c_p^{n-1}} \right)^{1/2} = \frac{G}{P^{n/2}} \lambda_o \quad . \tag{43}$$

We define the new variables,

$$y = \frac{dT}{d\eta}$$

and

$$\xi = T_f - T \quad .$$

Then equation (43) reduces to a first order differential equation.

$$\frac{dy}{d\xi} = -1 + \frac{\exp(-E/(T_f - \xi))}{\lambda^2 (T_f - \xi)^n} \frac{\xi^n}{y} \quad . \tag{44}$$

The boundary conditions of equation (44) are

$$y = 0 \qquad \text{at } \xi = 0$$

and

$$y = y_0 \qquad \text{at } \xi = T_f - 1 \quad .$$

The value of y_o is determined such that the gas and solid phase temperature profiles satisfy equation (30). If y_o is specified, λ is a "connecting coefficient" which satisfies two boundary conditions simultaneously in the solution of the first order differential equation (44). This gives us a functional relationship between y_o and λ, i.e., $y_o = f(\lambda)$. Two techniques were used to solve equation (44), a finite difference method and an asymptotic method.

Finite difference method. Assume the value of λ is given. We integrate equation (44) from $\xi = 0$ to $\xi = T_f - 1$ by a finite difference method. However, since the point $\xi = 0$, $y = 0$ is singular, the finite difference method fails in its vicinity. It is, therefore, necessary to find an asymptotic solution. In the vicinity of $\xi = y = 0$, equation (44) becomes,

$$\frac{dy}{d\xi} = -1 + B\frac{\xi^n}{y} \tag{45}$$

where

$$B = \exp(-E/T_f)/\lambda^2 T_f^n \quad .$$

Three different asymptotic solutions are obtained for different values of n.

a) $n < 1$.

In this case, $\xi^n/y \gg 1$, and equation (45) becomes

$$\frac{dy}{d\xi} = B \frac{\xi^n}{y} \quad .$$

The solution is,

$$y = \sqrt{\frac{2B}{n+1}} \; \xi^{\frac{n+1}{2}} \quad . \tag{46}$$

Consider the flame thickness.

$$x_f = \int \frac{dT}{y} \simeq \int \frac{d\xi}{y} = \int \xi^{\frac{n+1}{2}} \, d\xi = \xi^{\frac{1-n}{2}} \longrightarrow 0 \quad .$$

Hence, the temperature achieves its final value at a finite distance from the propellant surface.

b) $n = 1$.

In this case, $\xi^n/y \simeq 1$, and equation (45) becomes,

$$\frac{dy}{d\xi} = C \quad .$$

The solution is,

$$y = C \quad .$$

The constant C is determined by substituting $dy/d\xi = C$ and $y = C\xi$ into equation (45). The result is,

$$C = -0.5 + 0.5 \sqrt{1+4B} \quad .$$

Hence, the asymptotic solution is given by

$$y = \frac{-1 + \sqrt{1 + 4B}}{2} \; \xi \quad . \tag{47}$$

c) $n > 1$

The asymptote is given by a curve on which $dy/d\xi = 0$. Hence, the asymptote is,

$$y = B\xi^n \quad . \tag{48}$$

In the small interval $0 < \xi < \xi_1$, the solution is approximated by the asymptotic solutions. ξ_1 should be selected so that it is small enough so that the asymptotic solutions are good approximations, but large enough so that further integration can be performed by the finite difference method with a

reasonable step size. For $n < 1$, ξ_1 must be very small. From ξ_1 to $\xi = T_f - 1$, the equation was integrated by the Cutta-Runge method with automatic error control. The computations were performed for various values of λ and $\lambda \sim y_o$ relationships were obtained. A sample FORTRAN program is given in Appendix 1 for reference.

In the steady state, the solid phase temperature profile is given by the solution of equation (37). The result is,

$$T = T_i + (1-T_i)\, e^{\eta_s} \quad . \tag{49}$$

Hence, y_o is given by,

$$y_o = \frac{c}{c_p} \left.\frac{\partial T}{\partial \eta}\right|_{s,w} + \Delta h_w = \frac{c}{c_p} (1 - T_i) + \Delta h_w \quad . \tag{50}$$

Since λ is a function of y_o and hence a function of the propellant properties only, the steady state pressure burning rate relation is given by λ = constant. Hence,

$$G = P^{n/2} \quad . \tag{51}$$

Thus, the present model produces Viellie's steady state equation. If all thermodynamic properties, transport properties and chemical kinetic data were known, burning rates could presumably be calculated. However, burning rate data are more plentiful than kinetic data. We evaluate the value of the pre-exponential coefficient K by using,

$$K = \frac{\bar{G}_1^2 \bar{T}_w R^n \bar{h}^{on-1}}{\bar{P}_1^n \sqrt{g c_p^{n-1} \lambda_o^2}} \quad .$$

Using the property values listed in Table 1, K was evaluated for $n \neq 1$. The results are shown in Table 2.

TABLE 2

MAGNITUDE OF PREEXPONENTIAL TERM

IN THE RATE EQUATION, K

E	h_w	K(1/sec.)
5.56	-0.2	0.148×10^8
	0.	0.245×10^8
	0.2	0.347×10^8
11.12	-0.2	4.70×10^8
	0.	6.35×10^8
	0.2	8.15×10^8

They are in reasonable agreement with the values proposed by other investigators[15]. For reference the steady state temperature and concentration profiles in the gas phase for n = 1.0, E = 5.56 are shown in figure 1. The physical dimension was computed using property values in Table 1 and $\bar{G}_1 = 1.0$ g/sec. cm^2.

Asymptotic method. We seek the asymptotic solution for small values of λ. For a small value of λ, the flame is thin and y is large. Hence, $dy/d\xi \gg 1$. Then equation (44) is reduced to,

$$\frac{1}{2}\frac{d(y^2)}{d\xi} = \frac{\xi^n}{\lambda^2 (T_f-\xi)^n} \exp(-E/(T_f-\xi)) \quad . \tag{52}$$

Integrating equation (52) from $\xi = 0$ to ξ, one obtains,

$$y = (1/\lambda)\left(2\int_0^{\xi} \frac{\xi'^n}{(T_f-\xi')^n} \exp(-E/(T_f-\xi'))\, d\xi'\right)^{1/2} \tag{53}$$

It can thus be seen that $y \to 1/\lambda$ as $\lambda \to 0$. This suggests the following expansion:

$$y = (1/\lambda)(A_0 + A_1\lambda + A_2\lambda^2 + \ldots) \quad . \tag{54}$$

Substituting equation (54) into equation (44) and equating the same order terms of λ on the left and right hand sides, one obtains,

$$A_0 = \left[2\int_0^{\xi} \frac{\xi'^n}{(T_f-\xi')^n} \exp(-E/(T_f-\xi'))\, d\xi'\right]^{1/2} ,$$

$$A_1 = -\frac{\int_0^{\xi} A_0(\xi')d\xi'}{A_0(\xi)} ,$$

$$A_2 = \frac{-\int_0^{\xi} A_1(\xi')\, d\xi' - 0.5A_1^2(\xi)}{A_0(\xi)} ,$$

$$A_3 = \frac{-A_1(\xi)\, A_2(\xi) - \int_0^{\xi} A_2(\xi')\, d\xi'}{A_0(\xi)}$$

$$A_4 = \frac{-\int_0^{\xi} A_3(\xi')\, d\xi' - 0.5A_2(\xi) - A_1(\xi)\, A_3(\xi)}{A_0(\xi)} ,$$

etc.

If the integrations are performed from $\xi = 0$ to $\xi = T_f - 1 = \xi_o$, one obtains y_o.

$$y_o = (1/\lambda)[A_0(\xi_o) + A_1(\xi_o)\,\lambda + A_2(\xi_o)\,\lambda^2 + \ldots] \quad . \tag{55}$$

The asymptotic expansion was performed for small values of λ because the burning rates during depressurization were expected to be smaller than the steady state burning rates at the corresponding pressures. A sample FORTRAN program for the computation of $A_0(\xi_o)$, $A_1(\xi_o)$, etc., is given in Appendix 2. The asymptotic series (55) produced the best approximation when the first five terms were retained. Temperature profiles can be obtained if $d\eta/dT = 1/y$ is numerically integrated once with respect to ξ.

For most of our computations, the asymptotic method was used to obtain $\lambda \sim y_o$ relationships. The finite difference method was used to determine the number of terms which should be retained in equation (55) for the best approximation. The approximations were good in the range of our interest. The $\lambda \sim y_o$ relationships thus obtained are shown in Figures 2 and 3.

Combining equations (31) and (55), one obtains

$$\frac{c}{c_p}\left(\frac{\partial T}{\partial x}\right)_{s,w} = G y_o - G\,\Delta h_w \quad ,$$

$$= \frac{G}{\lambda}(A_0 + (A_1 - \Delta h_w)\,\lambda + A_2\lambda^2 + \ldots) \quad , \tag{56}$$

where A_0, A_1 etc. are evaluated at ξ_o.

Let

$$F(\lambda) = A_0 + (A_1 - \Delta h_w)\,\lambda + A_2\lambda^2 + \ldots \quad .$$

Then equation (56) may be written,

$$\frac{c}{c_p}\frac{\lambda_o}{P^{n/2}}\left(\frac{\partial T}{\partial x}\right)_{s,w} = F(\lambda) \quad . \tag{57}$$

Since $F(\lambda)$ is known, equation (57) can be solved for λ, if $\left(\frac{\partial T}{\partial x}\right)_{s,w}$ is given. Then the burning rate G can be computed by,

$$G = \frac{\lambda}{\lambda_o} P^{n/2} = G_r P^{n/2} \quad . \tag{58}$$

The relative burning rate G_r is the ratio of the transient burning rate to the

steady rate at the corresponding pressure.

We can now obtain a bit of useful information by considering an extreme case. Suppose that a motor were depressurized infinitely fast. Since the response in the solid is relatively slow, the temperature profile in the solid, and, hence $\frac{\partial T}{\partial x}\Big)_{s,w,}$ remain the same as they were in the initial state. A_0 is a positive number and $F(\lambda)$ decreases monotonically. Therefore, as the pressure decreases, λ must decrease. The transient burning rates are, therefore, smaller during depressurizations than the steady rates at corresponding pressures. The burning rate becomes zero when the chamber pressure reaches,

$$P_{q,max} = \left(\frac{c}{c_p}\lambda_o(1 - T_i)\frac{1}{A_0}\right)^{2/n} . \tag{59}$$

Solid Phase Equations

We seek the solution of equation (35) or (36). If G is a given function of time, a unique solution is obtainable without the boundary condition (31). We seek the solution of equation (35) or (36) with the appropriate function G which satisfies equation (31), hence equation (57). Several schemes can be used to solve this problem.

Finite difference method. Since equation (35) is a partial differential equation of the parabolic type, it can be solved numerically by the finite difference method step by step along the time coordinate. G has to be determined at each step by iteration. The explicit finite difference method requires a very small time interval for each step to ensure stability, especially when G becomes small. More than 10^3 steps are required to cover the pressure range from P = 1.0 to P = 0.01. The implicit method eliminates the stability problem and allows the use of larger time intervals, but requires a more elaborate iteration process.

Similar solution method. When G is given as a function of time, e.g.,

$$G = 1/(C_1 t + C_2)^{1/2} ,$$

equation (35) becomes an ordinary differential equation of the form,

$$f'' + (1 + 0.5C_1 D_s) f' = 0$$

where

$$\delta = f(\eta) , \quad \eta = -x/(C_1 t + C_2)^{1/2}, \quad \theta = (T - T_i)/(T_w - T_i) .$$

The solution is

$$f = A\int_0^{\eta} \exp\left(-\left(\eta + 0.25C_1 D_s \eta^2\right)\right) d\eta + 1 ,$$

$$A = -1/\int_o^\infty \exp\left(-\eta - 0.25 C_1 D_s \eta^2\right) d\eta \quad .$$

This solution satisfies the boundary conditions at $x = o$ and $x = -\infty$. The initial condition can be satisfied by putting $C_1 = 0$. It is possible to use this solution in the small interval and determine constants C_1 and C_2 so that equation (31) is satisfied at each time step. Different C_1 and C_2 must be used for each time interval. This procedure can be repeated to cover the necessary range of pressure, if the convergence of the process is proved.

Integral method. If the temperature profile in the solid changes smoothly with time, the integral method may produce a good approximation to the solution of equation (35). The temperature profile may be assumed in a polynomial form satisfying certain boundary conditions. For example, if one imposes the following boundary conditions

at $\eta = 0$, $\theta = 1$

at $\eta = 1$, $\theta = 0$

$\theta' = 0$

$\theta'' = 0$

one obtains,

$$\theta = 1 - 3\eta + 3\eta^2 - \eta^3 \qquad (*)$$

where

$$\theta(\eta) = (T - T_i)/(T_w - T_i), \quad \eta = -x/\delta(t).$$

From equation (57) and (*)

$$\delta = 3(1 - T_i)\frac{c}{c_p}\frac{\lambda_o}{p^{n/2}}\frac{1}{F(\lambda)} \qquad (**)$$

Eliminating t from equation (35) and (38) and integrating from $x = -\infty$ to $x = 0$, one obtains,

$$0.25\frac{D_s}{1 - r}(rG - P)\frac{d\delta}{dP} = \frac{P^{n/2}}{\lambda_o}\left(\frac{1}{1 - T_i}\frac{c_p}{c}F(\lambda) - \lambda\right) . \qquad (***)$$

Elimination of δ from equations (**) and (***) gives an ordinary differential equation for λ with respect to P. Instead of equation (*), one may use a non-similar temperature profile requiring satisfaction of equation (57) as a boundary condition. The disadvantage of the integral method is that the accuracy is known only when the result is compared with the exact solution.

Moving heat source method. This method is used in the present study to solve equation (36). With this method burning rates can be obtained without computing the temperature profiles in the solid. We solve equation (36) with a moving boundary. To satisfy the boundary condition at the moving propellant surface, moving heat sources are distributed along the trajectory of the surface on the $x \sim t$ plane (figure i). For convenience the direction of the x-coordinate is reversed so that the positive direction is directed toward the solid phase. The whole x-space ($-\infty$ to $+\infty$) is used.

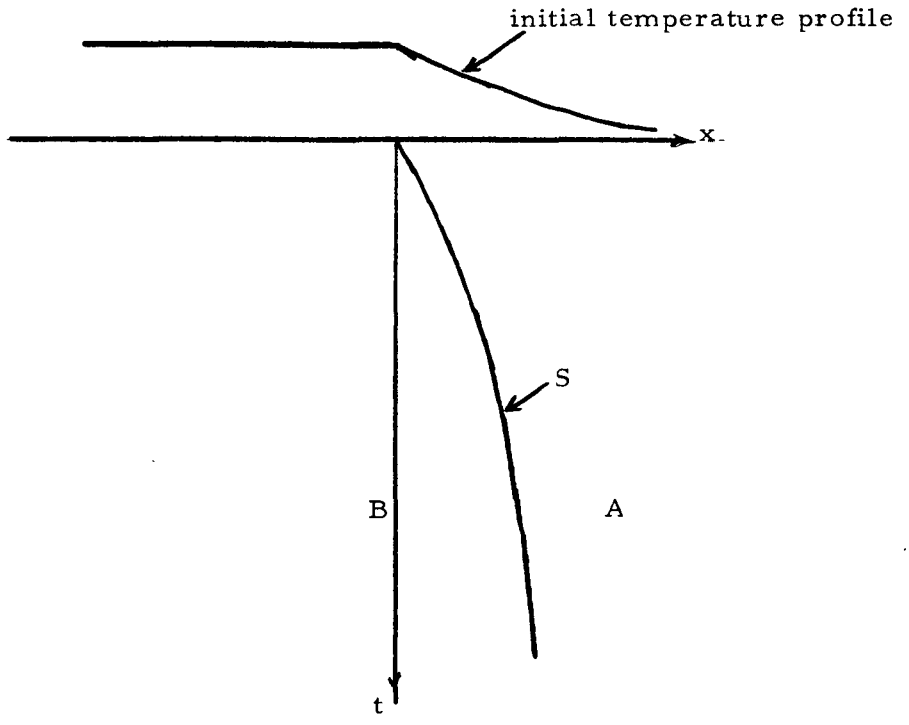

Figure i

We define the time and temperature scales:

$$\tau = t/D_s$$

and

$$\theta = \frac{T - T_i}{1 - T_i} \cdot$$

Equation (36) then becomes,

$$\frac{\partial \theta}{\partial \tau} = \frac{\partial^2 \theta}{\partial x^2} \tag{60}$$

with the boundary condition,

$$\theta = 1 \qquad \text{on S.}$$

The initial temperature profile in the whole x-space is given by,

$$\theta_o = e^{-x} \qquad \text{at } x > 0$$

$$\theta_o = 1 \qquad \text{at } x < 0$$

where θ_o in $x < 0$ is somewhat arbitrary. This choice has a certain advantage which will be explained later. The solution of equation (60) with initial data θ_o is given by,

$$\theta_a \int_{-\infty}^{\infty} \theta_o (x') \, K_1(x, x', \tau, 0) \, dx' \tag{61}$$

where

$$K_1(x, x', \tau, \tau') = \frac{e^{-\frac{(x-x')^2}{4(\tau-\tau')}}}{2\sqrt{\pi(\tau-\tau')}} \quad .$$

The result of integration is,

$$\theta_a = 0.5 + 0.5 e^{(\tau-x)} - 0.5 \operatorname{erf} \frac{x}{2\sqrt{\tau}} + e^{(\tau-x)} \operatorname{erf} \frac{2\tau - x}{2\sqrt{\tau}} \quad . \tag{62}$$

To satisfy a boundary condition on the propellant surface, i.e., $\theta = 1$ on S, a moving heat source with the strength $\phi(\tau)$ is distributed along S. If a point heat source $f(x, \tau)$ is distributed on the $x \sim \tau$ plane, the temperature profile is given by the solution of,

$$\frac{\partial \theta}{\partial \tau} - \frac{\partial^2 \theta}{\partial x^2} = f(x, \tau) \quad . \tag{63}$$

The solution is given by using Green's function. The result is given by,

$$\theta = \theta_a + \int K_1(x, x', \tau, \tau') \, f(x', \tau') \, dx' \, d\tau' \quad . \tag{64}$$

If the heat source is concentrated on the curve S, one may write.

$$f(x', \tau') = \phi(x', \tau') \, \delta(x', \tau') \tag{65}$$

where $\delta(x', \tau')$ is Dirac's delta function. Substituting equation (65) into (64), one obtains,

$$\theta = \theta_a + \int_o^\tau K_1(x, x', \tau, \tau')\, \emptyset\, (\tau')\ d\tau' \tag{66}$$

where (x', τ') is on curve S. Equation (64) satisfies equation (60) in $t > 0$, $-\infty < x < \infty$. except on S, where $\partial\theta/\partial x$ has a discontinuity. Integrating equation (63) from $x' - \varepsilon$ to $x' + \varepsilon$, and letting $\varepsilon \to 0$, and using equation (65), one obtains,

$$\emptyset(\tau') = -\left.\frac{\partial\theta\,(x', \tau')}{\partial x}\right)_+ + \left.\frac{\partial\theta(x', \tau')}{\partial x}\right)_- \tag{67}$$

where

$$\left.\frac{\partial\theta(x', \tau')}{\partial x}\right)_+ = \lim_{\varepsilon \to 0} \left.\frac{\partial\theta}{\partial x}\right)_{x = x' + \varepsilon}$$

and

$$\left.\frac{\partial\theta(x', \tau')}{\partial x}\right)_- = \lim_{\varepsilon \to 0} \left.\frac{\partial\theta}{\partial x}\right)_{x = x' - \varepsilon}^{\tau = \tau'}$$

However, $\theta = 1$ in domain B of figure 1. Hence,

$$\left.\frac{\partial\theta\,(x', \tau')}{\partial x}\right)_- = 0$$

and

$$\emptyset\ (\tau') = -\left.\frac{\partial\theta\ (x', \tau')}{\partial x}\right)_+ = \left.\frac{\partial\theta}{\partial x}\right)_{s, w} \tag{68}$$

Thus, the strength of the heat source is equal to the temperature gradient in the solid at the propellant surface. As was stated before, the distribution of θ_o in $x < 0$ and the position of the heat source are arbitrary. An advantage of our particular choice is the simple relationship between $\emptyset$ and $\left.\frac{\partial\theta}{\partial x}\right)_{s, w}$ expressed in equation (68). Along curve S, $\theta = 1$; hence, equation (64) becomes,

$$1 = \theta_a(x_s, \tau_s) + \int_o^{\tau_s} K_1(x_s, x', \tau_s, \tau')\, \emptyset\, (\tau')\ d\tau' \tag{69}$$

where points (x', τ') and (x_s, τ_s) are on S. The trajectory of the propellant surface is given by,

$$\frac{dx_s}{d\tau_s} = G(\tau_s), \quad \frac{dx'}{d\tau'} = G(\tau') \quad . \tag{70}$$

Equation (69) is an integral equation for $\emptyset$ (Voltera's integral equation of the 2nd kind) if G is a known function. G is determined such that $\emptyset$, hence, $\left.\frac{\partial\theta}{\partial x}\right)_{s, w}$ and G satisfy the surface energy balance equation (57) as well as equation (69). To do this, we approximate the time derivative and integral in equations (69) and (70) by finite difference equations and solve this equation

along the time coordinate. The procedure is described in the next section.

Numerical Procedures

At $\tau = 0$, $x_s = 0$, and $G = P = \phi = 1$. Suppose G, P, ϕ and x_s are known at τ_m. Denote $G(\tau_m)$, $P(\tau_m)$, $\phi(\tau_m)$ and $x_s(\tau_m)$ by G_m, P_m, ϕ_m, and $x_{s,m}$. Then G_{m+1}, P_{m+1}, ϕ_{m+1} and $x_{s,m+1}$ are determined in the following way.

Equation (69) is integrated in two parts, from $\tau = 0$ to $\tau = \tau_m$ and from τ_m to τ_{m+1}. The latter integral is approximated by,

$$\frac{\phi_m + \phi_{m+1}}{2} \int_{\tau_m}^{\tau_{m+1}} K_1(x_s, x', \tau_s, \tau')\, d\tau' \quad .$$

Assuming constant G from τ_m to τ_{m+1},

$$x_{s,m+1} = x_{s,m} + G_m \Delta\tau \tag{71}$$

Then the above integral is explicitly obtained as,

$$\frac{1}{G_m} \operatorname{erf}\left(T_m \sqrt{\Delta\tau}/2\right) \quad .$$

Equation (69) becomes,

$$\frac{\phi_m + \phi_{m+1}}{2} \frac{1}{G_m} \operatorname{erf}\left(G_m \sqrt{\Delta\tau}/2\right) = 1 - \theta_a(x_{s,m+1}, \tau_{s,m+1}) - \int_0^{\tau_m} K_1(x_{s,m+1}, x', \tau_{s,m+1}, \tau')\, \phi(\tau')\, d\tau' \quad . \tag{72}$$

The integral on the right hand side of (72) can be evaluated numerically. Then ϕ_{m+1} can be obtained from equation (72). P_{m+1} is given by the ballistic equation as,

$$P_{m+1} = P_m + \Delta P \quad .$$

$$\Delta P = \frac{D_s}{1-r} (rG - P)\, \Delta\tau \tag{73}$$

where

$$r = \left(\frac{P_2}{P_1}\right)^{1-m}$$

Combination of equations (57) and (68) gives,

$$\frac{c}{c_p}(1-T_i)(\phi_{m+1})\left(\frac{\lambda_o}{P^{n/2}_{m+1}}\right) = F(\lambda_{m+1}). \tag{74}$$

Since the right hand side of the equation (74) is a known function, equation (74) can be solved for λ_{m+1}. Then G_{m+1} is given by,

$$G_{m+1} = \frac{\lambda_{m+1}}{\lambda_o} P^{n/2}_{m+1} \tag{75}$$

In the actual computation, the solution of equation (74) for λ_{m+1} was simplified by a priori determining the inverse function of $F(\lambda)$ in a polynomial form by the least squares approximation. Thus,

$$\lambda_{m+1} = F^{-1}(a_{m+1}) \tag{74'}$$

where

$$a_{m+1} = \frac{c}{c_p}(1 - T_i)\,\phi_{m+1}\,\frac{\lambda_o}{P^{n/2}_{m+1}}$$

and

$$F^{-1}(a) = B_0 + B_1 a + B_2 a^2 + \ldots .$$

Ninth order polynomials were used for $F^{-1}(a)$ with satisfactory accuracy. To improve the accuracy of the computation, a predictor-corrector method was used. This method is briefly explained in the following paragraph.

First the procedure is applied to the interval between τ_m and $\tau_c = \tau_m + \Delta\tau/2$ to obtain $G_c = G(\tau_c)$, $P_c = P(\tau_c)$, $x_{s,c} = x_s(\tau_c)$ and $\phi_c = \phi(\tau_c)$. Then G_m in equation (71) and (72) is replaced by G_c. The computation of ΔP is improved by replacing P_m, G_m by P_c and G_c in equation (73). The rest of the procedure is exactly the same.

The evaluation of the integral

$$\int_o^{\tau_m} K_1(x_{s',m+1}, x', \tau_{m+1}, \tau')\,\phi(\tau')\,d\tau'$$

must be done with high accuracy, particularly in the vicinity of τ_m, because K_1 approaches infinity as τ' approaches τ_{m+1}. This integral was approximated by,

$$\sum_{n-1}^{m-1} \frac{\phi_n+\phi_{n+1}}{2} \int_{\tau_n}^{\tau_{n+1}} \frac{\exp\left[-\frac{\left(x_{m+1}-x_n-\frac{\Delta x}{\Delta\tau}(\tau'-\tau_n)\right)^2}{4(\tau_{m+1}-\tau')}\right]}{2\sqrt{\pi(\tau_{m+1}-\tau')}}\, d\tau \qquad (76)$$

where

$$\Delta x = x_{n+1} - x_n \ ,$$

and

$$\Delta\tau = \tau_{n+1} - \tau_n \ .$$

The integral in the above equation was evaluated by Romberg's method with a relative error less than 10^{-6} for each interval. One might suppose that the requirement of great accuracy is not justified since the approximation in the above equation with respect to ϕ may produce a larger error. However, one may interpret $(\phi_n + \phi_{n+1})/2$ to be the exact value of $\bar{\phi} = \phi(\tau_n + \Delta\tau)$, where $1 > a > 0$, such that,

$$\int_{\tau_n}^{\tau_{n+1}} K_1 \phi\, d\tau' = \phi \int_{\tau_n}^{\tau_{n+1}} K\, d\tau \ .$$

As the computation proceeds, $dP/d\tau$ becomes smaller. If the same time interval is used for the entire computation, undue computer time is used as P approaches zero. Therefore, in our computation a fixed ΔP was used and $\Delta\tau$ was computed by equation (73). To determine the size of ΔP which produces enouth accuracy, the computation was first carried out with error control on G. After the appropriate ΔP was established, the error control was removed for computer time economy. The FORTRAN program used for the computation is shown in Appendix 3.

Quench Limits

Quench limits can be obtained from burning rate computations. When the burning rate becomes zero at a non-zero chamber pressure, the motor is said to have quenched. If the burning rate becomes equal to the mass flow rate through the expanded nozzle, the chamber pressure starts to increase. The result is a burn-out. For a particular propellant the behavior of the burning rate depends only on D_s and P_2/P_1. The quench limit thus becomes a line on the $D_s \sim P_2/P_1$ plane. We call the value of D_s at the quench limit the critical depressurization parameter D_{sc}. D_{sc} is zero at $P_2/P_1 = 0$, and infinity at $P_2/P_1 = 1$.

Results. Input data for the computations done on a CDC 6600 digital computer are listed in Table 3. Comparison of problems I, II, and III gives the effects of the enthalpy of evaporation. Comparison of II and IV gives the effects of

the gas phase activation energy. Comparison of II, V and VI gives the effects of the gas phase reaction order or the pressure exponent of the steady state burning rate. Computations for larger values of P_2/P_1 are of little practical use because the depressurization rates needed to quench in such cases are so large that they can be achieved only with very small chamber free volumes. The burning rates were calculated in a series of computer experiments. From a given starting condition, the engine was depressurized at various rates, given by D_s, at each of a number of pressure ratios given by P_2/P_1 until a quench was observed. The computer time required for each "firing" was about three minutes. Approximately 20 runs were needed for each limit curve. Instability in numerical computations was experienced when D_s was small. In our computations, the pressure interval, ΔP, was fixed at .005. When D_s is small, the associated time interval is large. This causes a numerical instability. The critical depressurization parameter, D_{sc}, is small when n is large. If $n > 1.4$, a smaller pressure interval is required. Numerical instability also arises if the numerical integration of equation (76) is insufficiently accurate.

TABLE 3

INPUT DATA

Problem	n(or 2m)	E	H_w	P_2/P_1
I	1.0	5.56	-0.2	0.05, 0.1, 0.2
II	1.0	5.56	0.	0.05, 0.1, 0.2
III	1.0	5.56	+0.2	0.05, 0.1, 0.2
IV	1.0	11.12	0.	0.1, 0.2
V	1.2	5.56	0.	0.1, 0.2
VI	0.8	5.56	0.	0.1, 0.2

Computed transient burning rates are plotted against chamber pressure in Figures 4 through 18. The upper portions show the overall pictures. The lower portions show the detailed behavior near the end of the depressurization process. The distinction between a quench and a burn-out can be clearly seen. If a burn-out occurs, the computation stops when the burning rate curve reaches the nozzle mass flow rate curve. At this point, dP/dt becomes zero. The burning rate curve should thus be vertical on a $G \sim P$ plane. Our pressure interval was not small enough to show this trend.

Transient burning rates were always lower than steady burning rates at corresponding pressures. When D_s was large, the reduction was greater. The differences are small at the beginning of the depressurization; they become more pronounced as depressurization proceeds. Figure 19 shows this clearly.

Typical chamber pressure~time curves are shown in Figure 20. The physical time scale was computed from propellant data in Table 1 and $\bar{G}_1 = 1$ g/cm^{2}sec. In a burn-out, the chamber pressure will climb back up to P_2. The results indicate that the relative burning rate is smaller for a smaller value of P_2/P_1, a smaller value of Δh_w, a smaller value of E and a larger value of n.

These data were used to construct quench limit curves on the D_s~P_2/P_1 plane. The results are shown in Figures 21 through 26. Each point represents one computer experiment. The trend of the curves is as anticipated, i.e., the critical depressurization parameter D_{sc} (or depressurization rate) is zero at $P_2/P_1 = 0$ and infinity at $P_2/P_1 = 1$. For small values of P_2/P_1, D_{sc}'s are almost directly proportional to P_2/P_1.

The quench limit is determined by two factors. The first is the response of the solid to an imposed pressure disturbance. The second is the boundary condition imposed by the motor configuration. The effect of P_2/P_1 is found mainly in the second factor. All other things being equal, the critical depressurization parameter decreases as Δh_w decreases; the propellant is easier to quench when the surface reaction is exothermic. The critical depressurization parameter also decreases as the activation energy of the gas phase reaction decreases and as the reaction order increases. Dependence of D_{sc} on n is very strong. It should be kept in mind that D_s depends not only on dP/dt but also on $\bar{G}_1$. Therefore, it is sometimes misleading to say that a propellant is easier to quench, when D_{sc} is smaller. It should also be noted that when two propellants have different values of E but have the same value of $\bar{G}_1$, they are supposed to have different values of pre-exponential coefficients of the rate equation.

Discussion

Comparison with experiments. The present theory agrees with Ciepluch's[2] observation that burning rates during depressurizations are lower than steady rates at the same pressures.

The critical depressurization parameters computed at $P_2/P_1 = 0.1$ are in the range of 0.5~30. If we assume the values of ρ_s and Γ_s listed in table 1 and $\bar{G}_1 = 1.0$ g/cm^{2}sec. (a typical value at $\bar{P}_1 = 500$ psia), the corresponding critical depressurization rates P_1/t^* ($d\bar{P}/dt$ at the beginning of the pressure transient) are in the range 0.42×10^5~25×10^5 psi/sec. Experimentally observed[1,2] critical depressurization rates (defined by $\bar{P}_1/t_{1/2}$) are in the range of 0.5×10^5~2.0×10^5 psi/sec. If we consider the difference in the definition of depressurization rate and the fact that the values of P_2/P_1 in these experiments are probably lower than 0.1, the agreement is good.

Ciepluch[1] also reported that the critical depressurization rate is nearly proportional to the initial chamber pressure, and, therefore, the critical time is nearly independent of the initial pressure. His experiment used a motor whose depressurization rate was controled by varying the vent nozzle area.

Hence, P_2/P_1, $\overset{*}{t}$, and $\bar{P}_1$ are related.

$$\left(\frac{P_2}{P_1}\right)^{m-1} = 1 + C_1 \frac{V_c}{A_p} \frac{\bar{P}_1^{1-m}}{\overset{*}{t}} \tag{i}$$

where V_c is the chamber free volume, A_p is the propellant burning surface area and C_1 is a propellant constant. The definition of D_s is,

$$D_s = \frac{C_2}{\overset{*}{t}\,\bar{P}_1^{2m}} \tag{ii}$$

where C_2 is a propellant constant. Elimination of $\bar{P}_1$ from equations (i) and (ii) gives,

$$D_s = \frac{C_2 \left(\frac{C_1 V_c}{A_p}\right)^{\frac{2m}{1-m}}}{\left(\frac{1}{r} - 1\right)^{2m/(1-m)} \overset{*}{t}^{(1+m)/(1-m)}} \tag{iii}$$

where $r = (P_2/P_1)^{1-m}$. Equation (iii) gives the relation between P_2/P_1, D_s and $\overset{*}{t}$ when depressurization is imposed on the motor by a sudden opening of a vent. If we substitute $\overset{*}{t} = \overset{*}{t}_{crit.} = \text{const.}$ into equation (iii), it gives a limit curve on the $D_s \sim P_2/P_1$ plane which is consistent with Ciepluch's experiments. The result agrees with the results of this study (Fig. 27), but the present theory goes one step further. If the quench limit curves on the $D_s \sim P_2/P_1$ plane are obtained for the same propellant but with different motors, they fall on the same curve.

The trends of the effects of n, E and Δh_w on quench presented in this study cannot be adequately compared with experiments at present. Although effects of propellant composition have been studied[2], we don't know enough about the relationships between composition and physical and chemical properties. The present theory predicts a strong dependency of D_{sc} on n. Consider a quenching experiment in which two propellants with different values of n are tested with the same motor and at the same initial pressure. If we achieve the same depressurization rate for both propellants, the resulting P_2/P_1 will be larger for a propellant with a larger value of n,

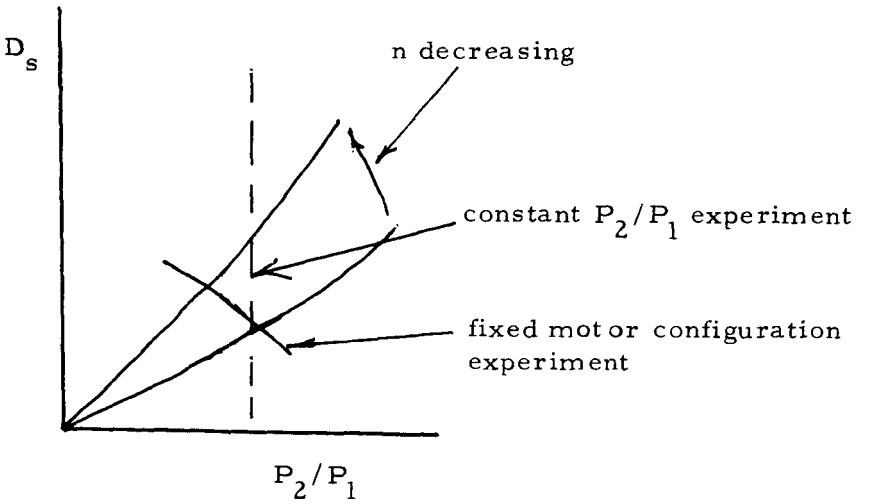

Figure ii

i.e., a high pressure dependence of the steady state burning rate makes a propellant easier to quench (figure ii).

No computation was performed for the case where the ambient pressure is not zero. In this case a nozzle mass flow rate curve on the G P plane intersects with P-axis. This tends to increase D_{sc}. Extinguishment will not be obtained if the ambient pressure is higher than $P_{q,max}$ in equation (59).

Although a limit curve plotted on the $\bar{P}_1$ $d\bar{P}/d\bar{t}$ plane is not uniquely determined by the propellant properties, and a curve plotted on the D_s P_2/P_1 plane is more general in the sense that it applies to all motor geometries, neither approach is necessarily appropriate if the depressurization rate is controled in a different manner, for example, by controling the opening rate. Thus, there is no unique quenching limit curve for a propellant.

Improvement of the present theory. One of the crucial assumptions in this study is that of constant surface temperature. The surface temperature probably decreases slightly as the burning rate decreases. If a functional relationship between the burning rate and the surface temperature is known, the present theory can accomodate this relationship with the following modifications.

We redefine $\overset{*}{T}$ to be the initial surface temperature. $\bar{T}_f$ is assumed to stay constant. Then y_o is a function of λ and $T_w(t)$. Equation (57) is replaced by,

$$\frac{c}{c_p}\,\frac{\lambda_o}{\rho^{n/2}}\left(\frac{\partial T}{\partial x}\right)_{s,w} = F(\lambda, T_w) \tag{1a}$$

The function $F(\lambda, T_w)$ must be a priori determined. It may be convenient to express F as $F = F_1(\lambda)F_2(T_w)$. To solve the solid phase equation (36), we use the same initial data shown in figure i. Since the temperature distribution in x 0 is no longer uniform equation (68) does not hold and $\left(\frac{\partial\theta(x', \tau')}{\partial x}\right)_-$ has to be evaluated. Differentiate equation (64) with respect to x at (x_s, τ_x). The result gives the arithmatic mean of $\left(\frac{\partial\theta}{\partial x}\right)_+$ and $\left(\frac{\partial\theta}{\partial x}\right)_-$. Thus,

$$0.5\left(\left(\frac{\partial\theta}{\partial x}\right)_+ + \left(\frac{\partial\theta}{\partial x}\right)_-\right) = \frac{\partial\theta a}{\partial x} - \int_0^{\tau_s} K_1(x_s, x', \tau_s, \tau')\,\frac{(x_s - x')}{2(\tau_s - \tau)}\,\phi(\tau')\,d\tau' . \tag{2a}$$

Combination of equations (2a) and (67) gives the value of $\left(\frac{\partial\theta}{\partial x}\right)_+$ at (x_s, τ_x).

Suppose the computation has been completed up to $\tau = \tau_m$. We continue the computation to $\tau_{m+1} = \tau_m + \Delta\tau$. Compute $\theta_{w,m+1}$ from,

$$\theta_{w,m+1} = f(G_m) \tag{3a}$$

where $\theta = f(G)$ is the surface temperature~burning rate relationship. Replace the first term (one) of the right hand side of equation (72) by θ_{m+1}. Compute $\phi(t_{m+1})$ in exactly the same way as we did with a constant surface temperature. Replace ϕ_{m+1} and $F(\lambda)$ by $\left(\frac{\partial\theta}{\partial x}\right)_+$ and $F(\lambda, T_w)$ in equation (74) and compute λ_{m+1}. The rest of the procedures are the same.

We did no computations involving varying surface temperature. However, we can speculate on the effect. No matter what form equation (3a) may take, experiments[16] suggest that θ_w is fairly constant up to a very small value of G. Suppose $\theta_w \simeq 0_{wo}$ up to $G = G_a$. Then the burning rate curve on the G~P plane will differ little from that for a constant surface temperature until $G = G_a$. If a burn-out results before G reaches G_a, both models predict almost the same burning rate behavior. If a burn-out does not occur at $G > G_a$, the burning rate beharior at $G < G_a$ may differ appreciably between the two models. However, if the criterion for a quench is established such that we regard the firing to be a quench if G becomes smaller than some arbitrary small value G_c, and if $G_c \simeq G_a$, the resulting quenching limits for both models are about the same.

Another major assumption made here is that there is no chemical reaction in the solid. It is quite likely that there are reactions in the solid, especially if the burning rate is low. If a significant solid phase reaction occurs near the propellant surface, we may treat it as a surface reaction in an analytical model. We have considered exothermic, neutral and endothermic surface reactions in our treatment. This may account partly for the effects of solid phase reactions.

Finally, we have made the assumption of a constant adiabatic flame temperature. Actually, during the pressure transient, the flame temperature will decrease somewhat because of redistribution of thermal energy within the combustion wave to produce a flatter profile in the solid. Consideration of this effect would make quenching somewhat easier than is suggested by our results.

SYMBOLS

A_t	primary nozzle throat area
A_v	vent nozzle throat area
c	specific heat capacity of propellant
c_p	specific heat capacity of the gas at constant pressure
D	diffusion coefficient
D_g	nondimensional parameter defined on page 10
D_s	depressurization parameter defined on page 12
e	internal energy
E	nondimensional activation energy in the gas phase
G	nondimensional burning rate (mass flow rate/area)
G_r	relative burning rate defined by equation (58)
h	enthalpy
k	thermal conductivity
K	pre-exponential coefficient in the rate equation
L_e	Lewis number
m	pressure exponent of steady state burning rate
m_i	mass concentration of i's species
$\dot{m}_t$	mass flow rate through the primary nozzle
$\dot{m}_v$	mass flow rate through the vent nozzle
P	nondimensional pressure
$\bar{P}_a$	ambient pressure
$\bar{P}_2$	steady state burning pressure corresponding to $A_t + A_v$
R	gas constant
r	$(P_2/P_1)^{1-m}$
t	nondimensional time
T	nondimensional temperature
$\bar{T}_i$	propellant ambient temperature
V_c	chamber free volume
x	nondimensional space coordinate
τ	t/D_x

θ nondimensional temperature defined on page 24

ϕ nondimensional strength of heat source

$k/c_{(p)}$

ρ density of the gas

ρ_s density of the propellant

γ specific heat ratio

λ defined on page 17

λ_o λ at $t = 0$

Δh^o enthalpy change in gas phase reaction (nondimensional)

Δh_w enthalpy change in surface reaction (nondimensional)

Superscripts and Subscripts

1 initial value

s solid phase

g gas phase

w propellant surface

- dimensional quantities

* nondimensionalizing quantities

APPENDIX 1. A SAMPLE FORTRAN PROGRAM FOR SOLVING THE GAS PHASE EQUATION BY A FINITE DIFFERENCE METHOD

Symbols

Y	= y
YPRIME	= $dy/d\xi$
S	= ξ
TIN	= T_f
ACT	= E
CON	= $1/\lambda^2$
RK	= library subroutine for Cutta-Runge method
Z	= n

```
C     N = 1,              E = 5.56

DIMENSION  Y(1), Y PRIME (1), ERR1 (1), W(4)
COMMON CON, TIN, ACT
EXTERNAL DERIV
TANF (CON, TIN, ACT) = -0.5+0.5*SQRTF(1.+4.*CON/TIN*EXPF(-ACT/TIN))
PRIME F(S, Y, CON, TIN, ACT)=-1.+S/Y*CON/(TIN-S)*EXPF(-ACT/(TIN-S))
ERR1 (1) = 1.E-9
ERR2 = 1.E-9
NUMBER = 1
H = 0.02
TIN = 3.
ACT = 5.56
DO 21 I = 1, 60
P = I
CON = 60.+20.*P+1.35*P*(P-1.)/2.
B1 = H*TANF(CON, TIN, ACT)
B2 = H*PRIMEF(H/2., B1/2., CON, TIN, ACT)
B3 = H*PRIMEF(H/2., B2/2., CON, TIN, ACT)
B4 = H*PRIMEF(H, B3, CON, TIN, ACT)
```

```
Y(1) = 1./6.*(B1+2.*B2+2.*B3+B4)
S = 0.02
SFINAL = 0.04
INIT = 1
CALL RK(S, SFINAL, Y, YPRIME, DERIV, NUMBER, ERR2, ERR1, INIT, W, DX)
INIT = -1
DO21 J = 1, 98
SFINAL = S+0.02
CALL RK(S, SFINAL, Y, YPRIME, DERIV, NUMBER, ERR2, ERR1, INIT, W, KX)
IF(J-98) 30, 31, 32
30  GO TO 21
31  PRINT 40, CON, y(1)
40  FORMAT (2E20.8)
    GO TO 21
32  GO TO 21
21  CONTINUE
    END
    SUBROUTINE DERIV(S, Y, YPRIME)
    DIMENSION Y(1), YPRIME(1)
COMMON CON, TIN, ACT
YPRIME(1) = -1.+S/Y(1)*CON/(TIN-S)*EXPF(-ACT/(TIN-S))
RETURN
END
END
```

APPENDIX 2. A SAMPLE FORTRAN PROGRAM FOR SOLVING THE GAS PHASE EQUATION BY THE ASYMPTOTIC METHOD

Symbols

YO = A_O

.

.

Y4 = A_4

ACT = E

TIN = T_f

Z = n

ROM2F = library subroutine for numerical integration

```
C     N = 1,            E = 5.56
      DIMENSION Y(5,501),R(500)
      EXTERNAL FUNEV
      Y(1,1) = 0.
      Y(2,1) = 0.
      Y(3,1) = 0.
      Y(4,1) = 0
      Y(5,1) = 0
      SUMR = 0.
      Z = 1.
      DO 2 I = 1,500
      P = I
      BOW = .004*(P-1.)
      UPP = .004*P
      CALL ROM2F(FUNEV, BOW, UPP, 0.001, NN, VAL)
      R(I) = VAL
      SUMR = SUMR + R(I)
    2 Y(1,I + 1) = SQRTF(SUMR)
      YO = Y(1,501)
```

```
      SUMR = 0.
      DO 3 I = 1,500
      R(I) = 0.002*(Y(1,I) + Y(1,I+1))
      SUMR =  SUMR +R(I)
3     Y(2,I+1) = 1.*SUMR/Y(1,I+1)
      Y1 = Y(2,501)
      SUMR = 0.
      DO 4 I = 1,500
      R(I) = 0.002*(Y(2,I)+Y(2,I+1))
      SUMR = SUMR + R(I)
4     Y(3,I+1) = (-0.5*Y(2,I+1)**2-SUMR)/Y(1,I+1)
      Y2 = Y(3,501)
      SUMR = 0.
      DO  5  I = 1,500
      R(I) = 0.002*(Y(3,I)+Y(3,I+1))
      SUMR = SUMR+R(I)
5     Y(4,I+1) = (-Y(2,I+1)*Y(3,I+1)-SUMR)/Y(1,I+1)
      Y3 = Y(4,501)
      SUMR = 0.
      DO  6  I = 1,500
      R(I) = 0.002*(Y(4,I)+Y(4,I+1))
      SUMR = SUMR+R(I)
6     Y(5,I+1) = (-SUMR-0.5*Y(3,I+1)**2-Y(2,I+1)* Y(4,I+1))/Y(1,I+1)
      Y4 = Y(5,501)
      PRINT 7,  YO Y1, Y2, Y3, Y4
7     FORMAT(5E20.8)
      END
      FUNCTION FUNEV(X)
      ACT = 5.56
      TIN = 3.
      Z = 1.
      FUNEV = 2.*X**Z/(TIN-X)**Z*EXPF(-ACT/(TIN-X))
      RETURN
      END
      END
```

APPENDIX 3. A SAMPLE FORTRAN PROGRAM FOR THE BURNING RATE COMPUTATIONS

The program consists of the main program, subroutine STEP, subroutine RV and function FX. The computation from P = 1.0 to 0.98 is done in the main program. The computation from $0.98-n\Delta P$ to $0.98-(n+1)\Delta P$, n = C, 1, 2, , is done in subroutine STEP. After the first step, the function of the main program is to check the output of STEP and stop the computation if a quench or a burn-out is reached. The criteria for a quench and a burn-out are: $G < 0.002$ for a quench, $dP/d\tau > -0.002$ for a burn-out. The subroutine RV computes λ from equation (74'). The integral (76) is evaluated by library subroutine ROM1F. The function FX represents the function K_1 in a small interval.

Symbols

N	= number of steps
T	= τ
X	= x
G	= G
P	= P
DT	= dt
DX	= dx
DG	= dG
DP	= dP
BETA	= G_r
PHI	= $\emptyset$
RN	= n
RM	= m
RAMDA	= λ
RAMDAS	= λ_o
TETF	= K_1
DELF	= $dP/d\tau$
RESF	= $1 - \theta_a$
ROM1F	= library routine for numerical integration

A sample FORTRAN program for a burning rate computation

```
C     N = 1.0       E = 5000°K,      HS = 0.
DIMENSION X(200), T(200), P(200), PHI(200), BETA(200), G(200)
COMMON DS, SR, RM, RAMDAS, TA, TB, XM, TM, XA, XB
EXTERNAL FX
DELF(DS, SR, P, G, ) = DS/(1. -SR)*(SR*G-P)
TETF(X, XO, T, TO, PAI) = EXPF(-1.*(X-XO)**2/4. /(T-TO))/2.
1/SQRTF(PAI*(T-TO))
RESF(X, T) = 0.5-0.5*EXPF(T-X)+0.5*(ERFN(X/2. /SORTF(T))
1+EXPF(T-X)*ERFN((2.*T-X)/2. /SQRTF(T)))
PAI=3.1415926535
RN = 1.0
RM = RN/2.
RAMDAS = .21759453
P(1) = 1.0
G(1) = 1.0
T(1) = 0.0
PHI(1) = 1.0
X(1) = 0.0
PR = 0.1
SR = PR**(1. -RM)
DS = 1.0
DP = -0.02
DP1 = 0.5*DP
DT1 = -DP1/DS
T1 = DT1
P1 = 1.0+DP1
CALL RV(1., P1, RAMDA)
G1 = RAMDA/RAMDAS*P1**RM
DT = DP/DELF(DS, SR, P1, G1)
X(2) = G1*DT
P(2) = 1.0+DP
T(2) = DT
RES = RESF(X(2), T(2))
DSUM = 1. /G1*ERFN(G1*SQRTF(T(2))/2.)
```

```
      PHI(2) = RES/DSUM*2.0-1.0
      CALL RV(PHI(2), P(2), RAMDA)
      BETA(2) = RAMDA/RAMDAS
      G(2) = BETA(2)*P(2)**RM
      N = 2
      PRINT 5, N, P(2), G(2),    T(2), BETA(2)
    5 FORMAT(I6, 4E20.8)
      DP = -0.005
   11 NINT = N
      IF(197-NINT) 22, 21, 20
   20 GO TO 23
   21 GO TO 500
   22 GO TO 500
   23 CALL STEP (N, T, P, X, G, PHI, BETA, DP, DPT)
      PRINT 5, N, P(N), G(N), T(N), BETA(N)
      IF(G(N)-0.002)   30, 30, 31
   30 PQ = P(N)-G(N)*(P(N)-P(N-1))/(G(N)-G(N-1))
      PRINT 70, PQ
   70 FORMAT(4H PQ = E20.8)
      GO TO 500
   31 GO TO 32
   32 REMAIN = -0.002DPT
      IF(REMAIN) 1, 1, 3
    1 SL = 1./SR
      SG = (G(N)-G(N-1))/(P(N)-P(N-1))
      GB = (G(N)-SG*P(N))/(1.0-SG/SL)
      PB = GB/SL
      PRINT 71, GB, PB
   71 FORMAT (4H GB = E20.8, 4H PB = E20.8)
      GO TO 500
    3 GO TO 11
  500 CONTINUE
      END
      SUBROUTINE STEP(N, T, P, X, G, PHI, BETA, DP, DPT)
```

```
      DIMENSION X(200(, T(200), G(200), P(200),  PHI(200), BETA(200)
      COMMON DS, SR, RM, RAMDAS, TA, TB, XM, TM, XA, XB
      EXTERNAL FX
      DELF(DS, SR, P, G) = DS/(1. -SR)*(SR*G-P)
      OTETF(X, XO, T, TO, PAI) = -EXPF(-1. *(X-XO)**2/4. /(T-TO))/2. /
     1SQRTF(PAI*(T-TO))
      ORESF(X, T) = 0.5-0.5*EXPF(T-X)+0.5*(ERFN(X/2. /SQRTF(T))+
     1EXPF(T-X)*ERFN((2. *T-X)/2. /SQRTF(T)))
      PIA = 3.1415926535
      DPT = DELF(DS, SR, P(N), G(N))
      IF(DPT)  10, 500, 500
10    DP1 = 0.5*DP
      DT1 = DP1/DPT
      DX1 = DT1*G(N)
      T1 = T(N)+DT1
      X1 = X(N)+DX1
      P1 = P(N)+DP1
      RES1 = RESF(X1, T1)
      M = N-1
      IF(N-2)  500, 4, 5
4     TA = T(1)
      TB = T(2)
      XA = X(1)
      XB = X(2)
      TM = T1
      XM = X1
      VAL = ROM1F(FX, TA, TB, 9)
      SUM = VAL*(PHI(1)+PHI(2))/2.
      GO TO 6
5     MM = M-1
      SUM = 0.
      DO 1 I = 1, MM
      TA = T(I)
```

```
      TB = T(I+1)
      XA = X(I)
      XB = X(I+1)
      TM = T1
      XM = X1
      VAL = ROM1F(FX, TA, TB, 5)
    1 SUM = SUM+VAL*(PHI(I)+PHI(I+1))/2.
      TA = T(M)
      TB = T(N)
      XA = X(M)
      XB = X(N)
      TM = T1
      XM = X1
      VAL = ROM1F(FX, TA, TB, 8)
      SUM = SUM+VAL*(PHI(M)+PHI(N))/2.
    6 DSUM = 1./G(N)*ERFN(G(N)*SQRTF(DT1)/2.)
      PHI1 = (RES1-SUM)/DSUM*2.-PHI(N)
      CALL RV(PHI1, P1, RAMDA)
      G1 = RAMDA/RAMDAS*R1**RM
      DT = DP/DELF(DS, SR, P1, G1)
      IF(DT) 11, 11, 12
   11 DPT = 0.
      GO TO 500
   12 DX = DT*G1
      T(N+1) = T(N)+DT
      X(N+1) = X(N)+DX
      P(N+1) = P(N)+DP
      RES = RESF(X(N+1), T(N+1))
      IF(N-2) 500, 7, 8
    7 TA = T(1)
      TB = T(2)
      XA = X(1)
      XB = X(2)
```

```
      TM = T(3)
      XM = X(3)
      VAL = ROM1F(FX, TA, TB, 8)
      SUM = VAL*(PHI(1)+PHI(2))/2.
      GO TO 9
    8 MM = M-1
      SUM = 0.
      DO 2 I = 1, MM
      TA = T(1)
      TB = T(I+1)
      XA = X(I)
      XB = X(I=1)
      TM = T(N+1)
      XM = X(N+1)
      VAL = ROM1F(FX, TA, TB, 5)
    2 SUM = SUM+VAL*(PHI(I)+PHI(I+1))/2.
      TA = T(M)
      TB = T(N)
      XA = X(M)
      XB = X(N)
      TM = T(N+1)
      XM = X(N+1)
      VAL = ROM1F(FX, TA, TB, 8)
      SUM = SUM+VAL*)PHI(M)+PHI(N))/2.
    9 DSUM = 1./G1*ERFN(G1*SQRTF(DT)/2.)
      PHI(N+1) = (RES-SUM)/DSUM*2.-PHI(N)
      CALL RV(PHI(N+1), P(N+1), RAMDA)
      BETA(N+1) = RAMDA/RAMDAS
      G(N+1) = BETA(N+1)*P(N+1)**RM
      N = N+1
  500 RETURN
      END
      SUBROUTINE RV(PH, P, RAM)
      COMMON DS, SR, RM, RAMDAS, TA, TB, XM, TM, XA, XB
```

```
Z = PH*0.4*RAMDAS/P**RM
AO = 0.49806528E+01
A1 = -0.28204058E+03
A2 = 0.75147485E+04
A3 = -0.11617785E+06
A4 = 0.11375420E+07
A5 = -0.73028185E+07
A6 = 0.30725407E+08
A7 = -0.81693743E+08
A8 = 0.12457777E+09
A9 = -0.83034562+08
RAM = AO+A1*Z+A2*Z**2+A3*Z**3+A4*Z**4+A5*Z**5+A6*Z**6+
1A7*Z**7+A8*Z**8+A9*Z**9
RETURN
END
FUNCTION FX(TO)
COMMON DS, SR, RM, RAMDAS, TA, TB, XM, TM, XA, XB
PAI = 3.1415926535
FX = EXPF(-1.*(XM-XA-(XB-XA)/(TB-TA)*(TO-TA))**2/4./(TM-1TO))
/2./SQRTF(PAI*(TN-TO))
RETURN
END
END
```

REFERENCES

1. Ciepluch, C., "Effect of rapid pressure decay on solid propellant combustion" ARS J. Vol. 31, 1584-1586 (1961).

2. Ciepluch, C., "Effect of composition on combustion of solid propellants during a rapid pressure decrease" NASA TN D-1559.

3. Kalt, S., "Thrust termination in solid propellant rocket motors-evaluation of ballistic test data" ARS J. Vol. 31 84-86 (1961).

4. Von Elbe, G., "Theory of solid propellant ignition and response to pressure transients" Bulletin of 18th ICRPG meeting.

5. Paul, B.E., Lovine, R.L., Fong, L.Y., "A ballistic explanation of the ignition peak" AIAA preprint No. 64-121.

6. Hiroki, T., "Combustion in solid propellant rocket motors undergoing depressurization to produce a quench" M.S. Thesis submitted to the University of Minnesota (1965).

7. Denison, M.R., Baum, E., "A simplified model of unstable burning in solid propellants" ARS J. Vol. 31, No. 8 (1961).

8. Capener, E.L., Dickinson, L.A., Marxman, G.A., "Propellant combustion phenomenon during rapid depressurization" Quarterly report No. 1, 2, 3, prepared by Stanford Research Institute.

9. Anderson, F.A., Strehlow, R.A., Strand, L.D., "Low pressure extinction" AIAA J. Vol. 1, 2669-2671 (1963).

10. Coates, R.L., Cohen, N.S., Harvill, L.R., "Interpretation of L* combustion instability in terms of acoustic instability theory".

11. Coates, R.L., Cohen, N.S., "Correlation of solid propellant extinguishment data" CPIA Pub. 118 (1965).

12 Coates, R.L., Polzien, R.E., Price, C.F., "Design procedure for combustion termination by nozzle area variation" J. of Spacecraft and Rockets, Vol. 3, No. 3 (1966).

13. Ciepluch, C., "Spontaneous reignition of previously extinguished solid propellants" NASA TN D-2167 (1964).

14 Patch, D.F., "The reignition response of a solid propellant to variation in chamber gas composition and temperature", M.S. Thesis submitted to the University of Minnesota (1967).

15. Friedman, R., "Research on solid propellant combustion" Final report for Contract AF 49(638)-813, Atlantic Research Co.

16. Sabadell, A.J., Wenograd, J., Summerfield, M., "Measurement of temperature profiles through solid-propellant flames using fine thermocouples" AIAA J. Vol. 3, No. 9 (1965).

17. Medford, J.E., "Measurement of thermal diffusivity of solid propellant" ARS J. Vol. 32, No. 9 (1962).

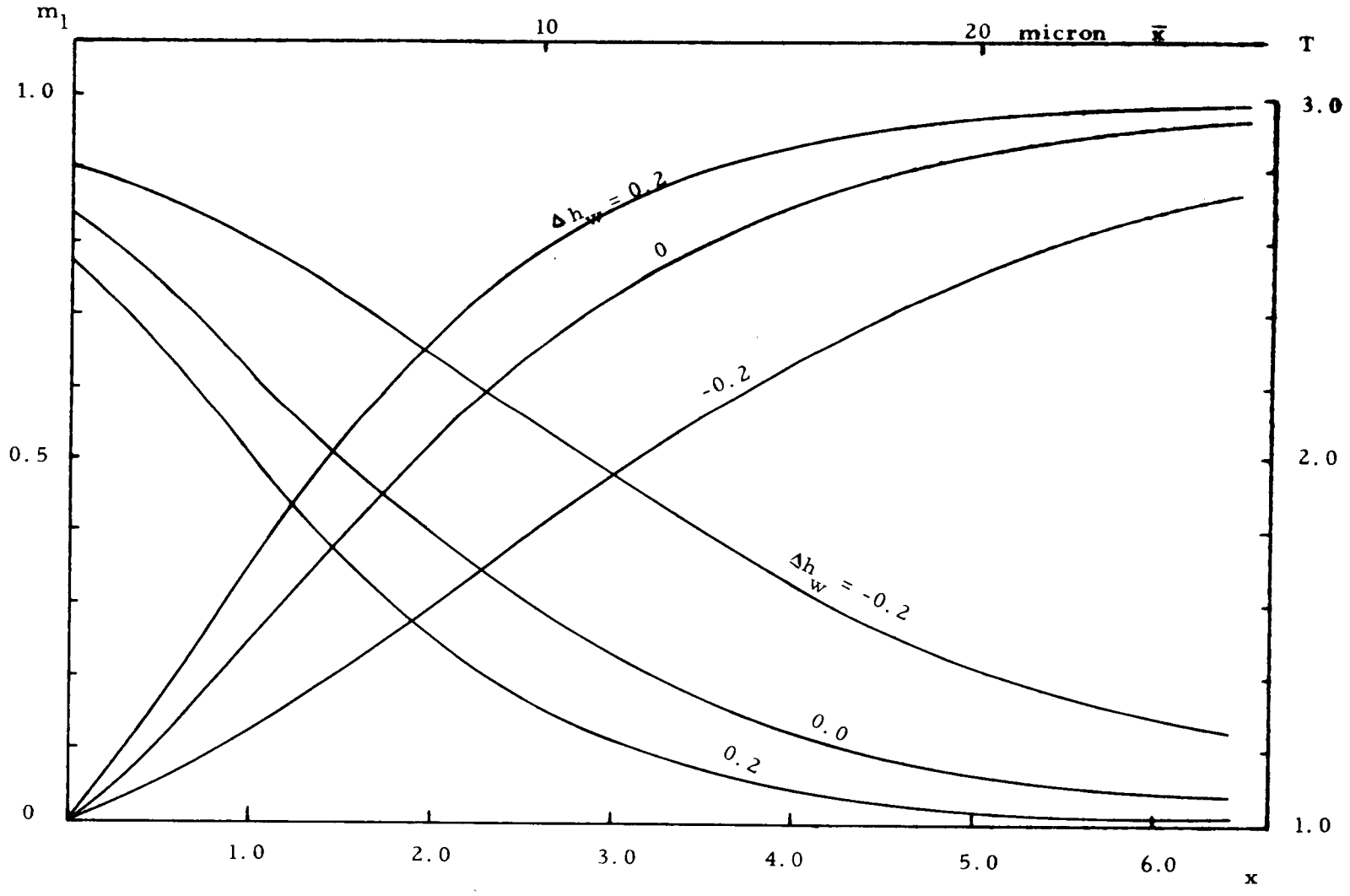

Figure 1. Steady state gas phase temperature profiles and their dependence on heat of vaporization of the propellant; n = 1.0, E = 5.56.

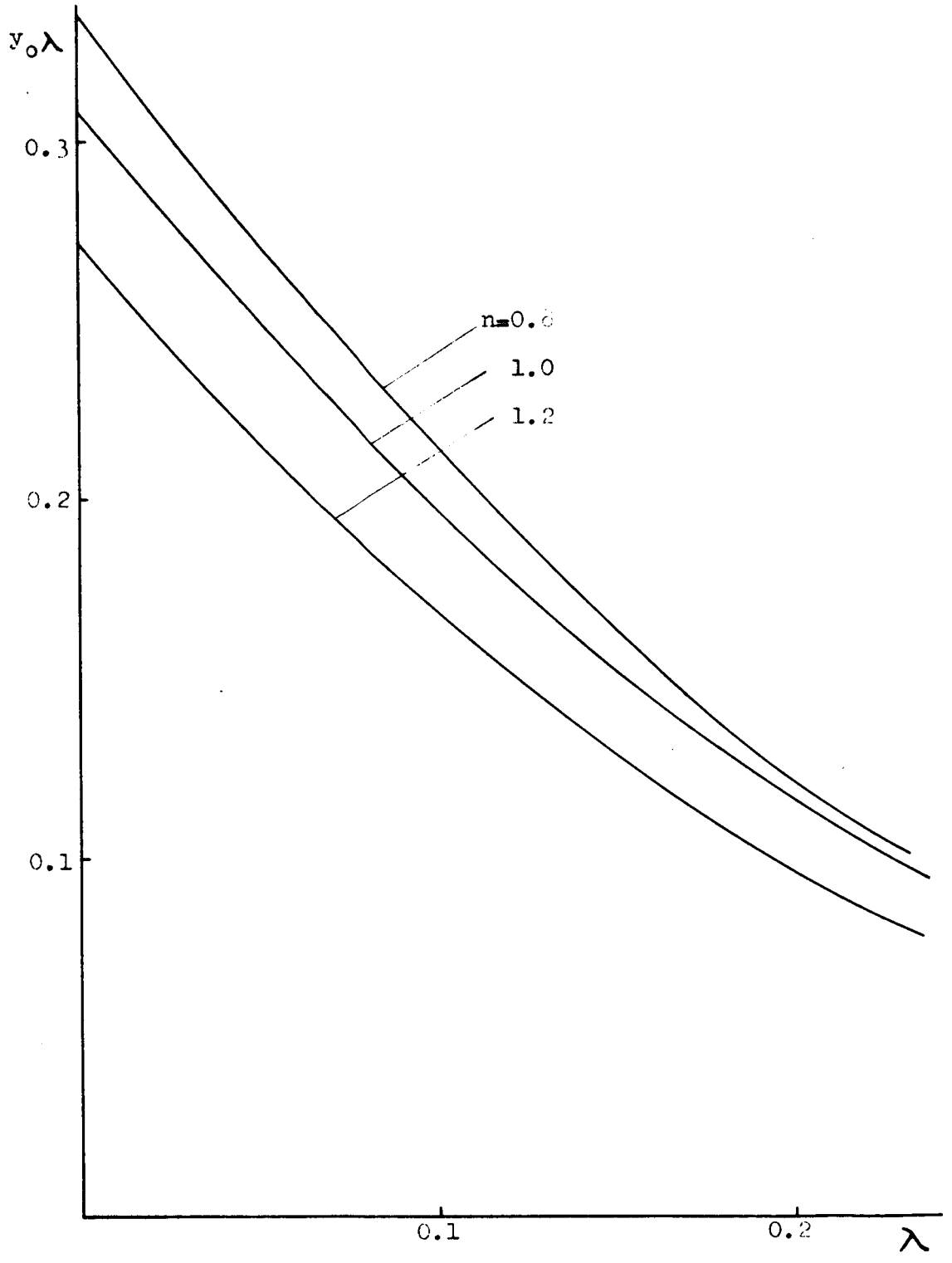

Figure 2. Variation of y_o with λ for various values of n; E = 5.56.

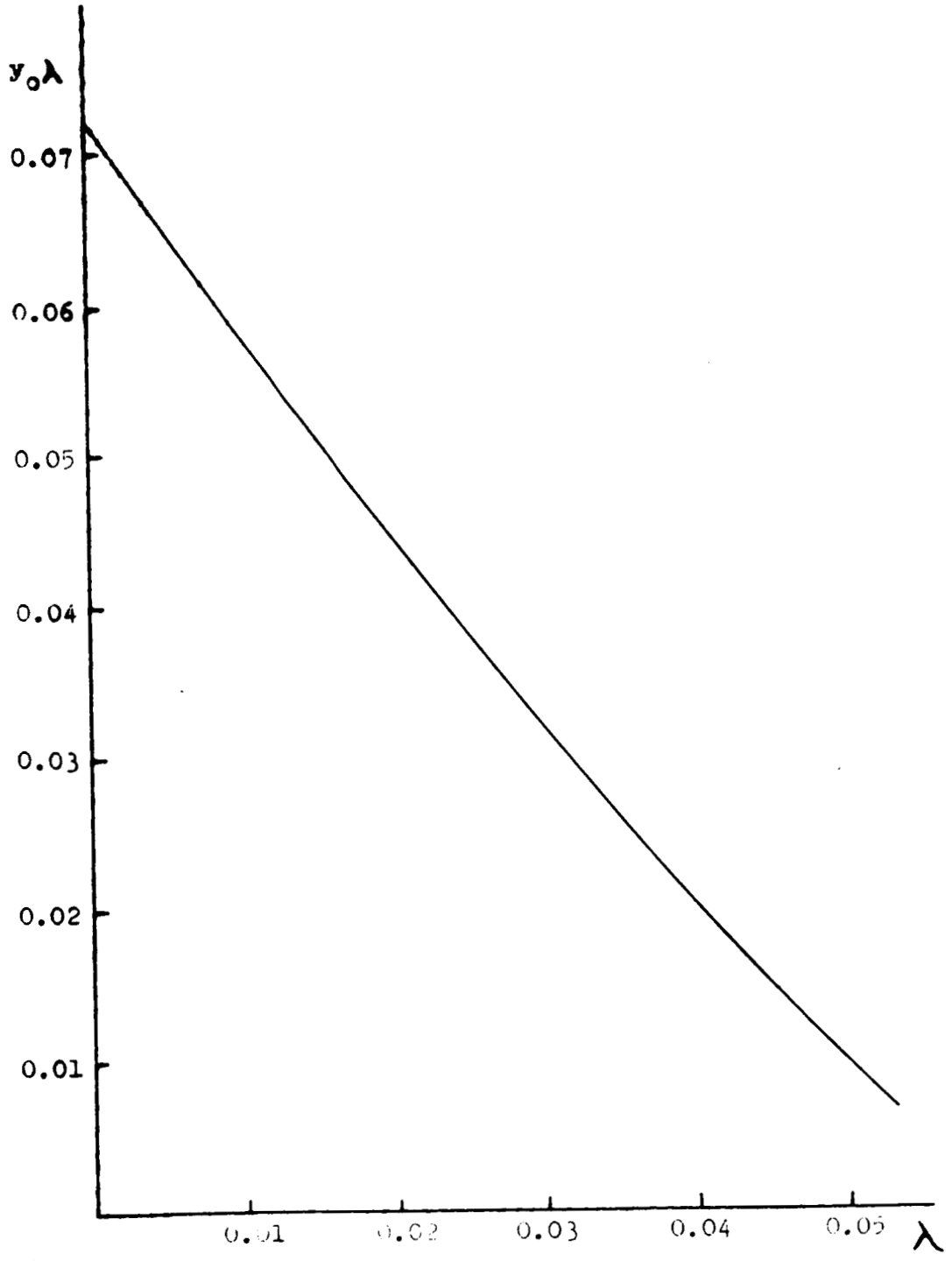

Figure 3. Variation of y_o with λ; n = 1.0, E = 11, 12.

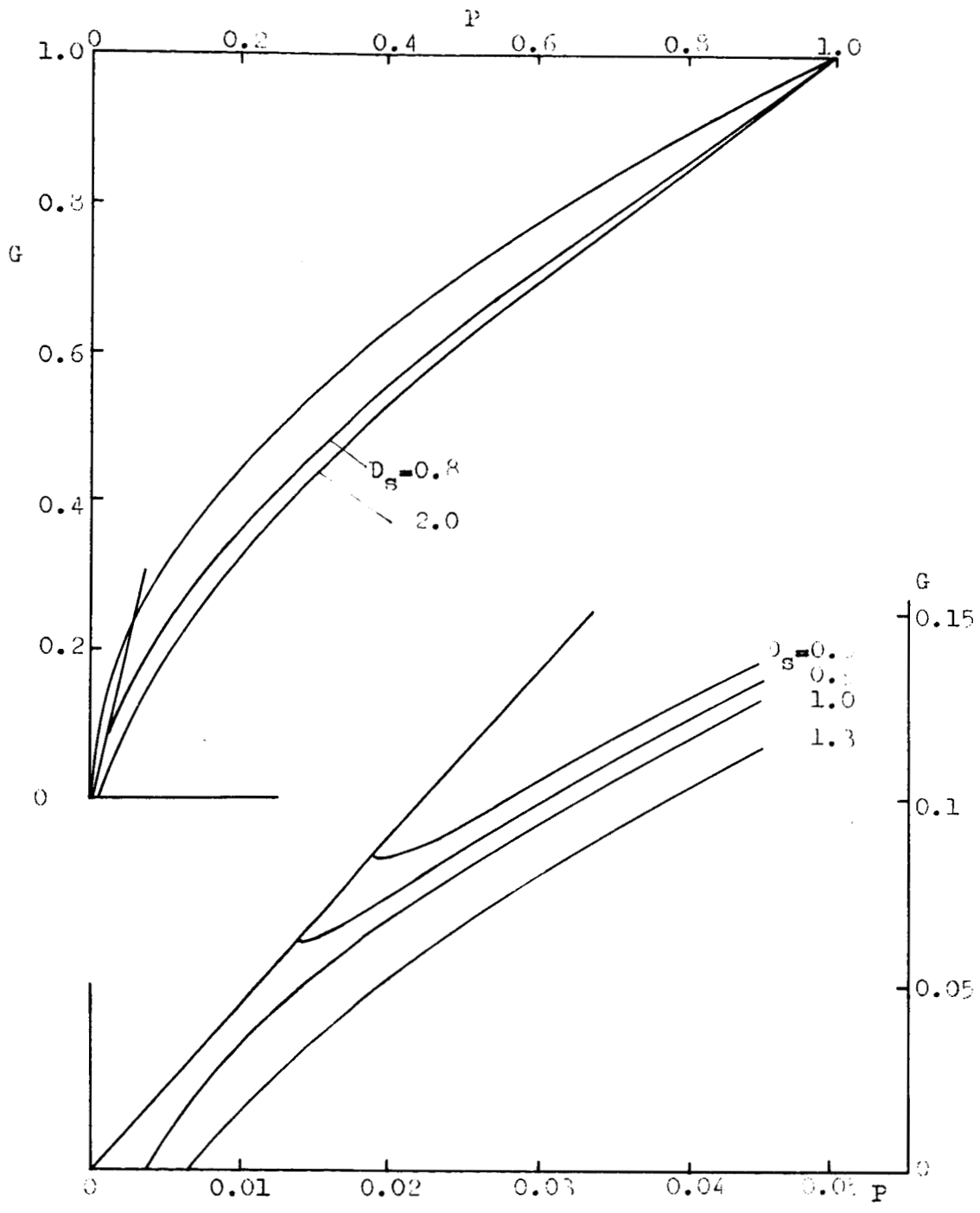

Figure 4. Variation of burning rate with pressure during depressurization at various depressurization rates. The upper part of the figure shows the gross effect. The lower part is a detailed view of the lower left hand corner. The straight line originating at the origins is the mass flux through the expanded nozzle. n = 1, E = 5.56, $\Delta h_w = 0$, $P_2/P_1 = 0.05$.

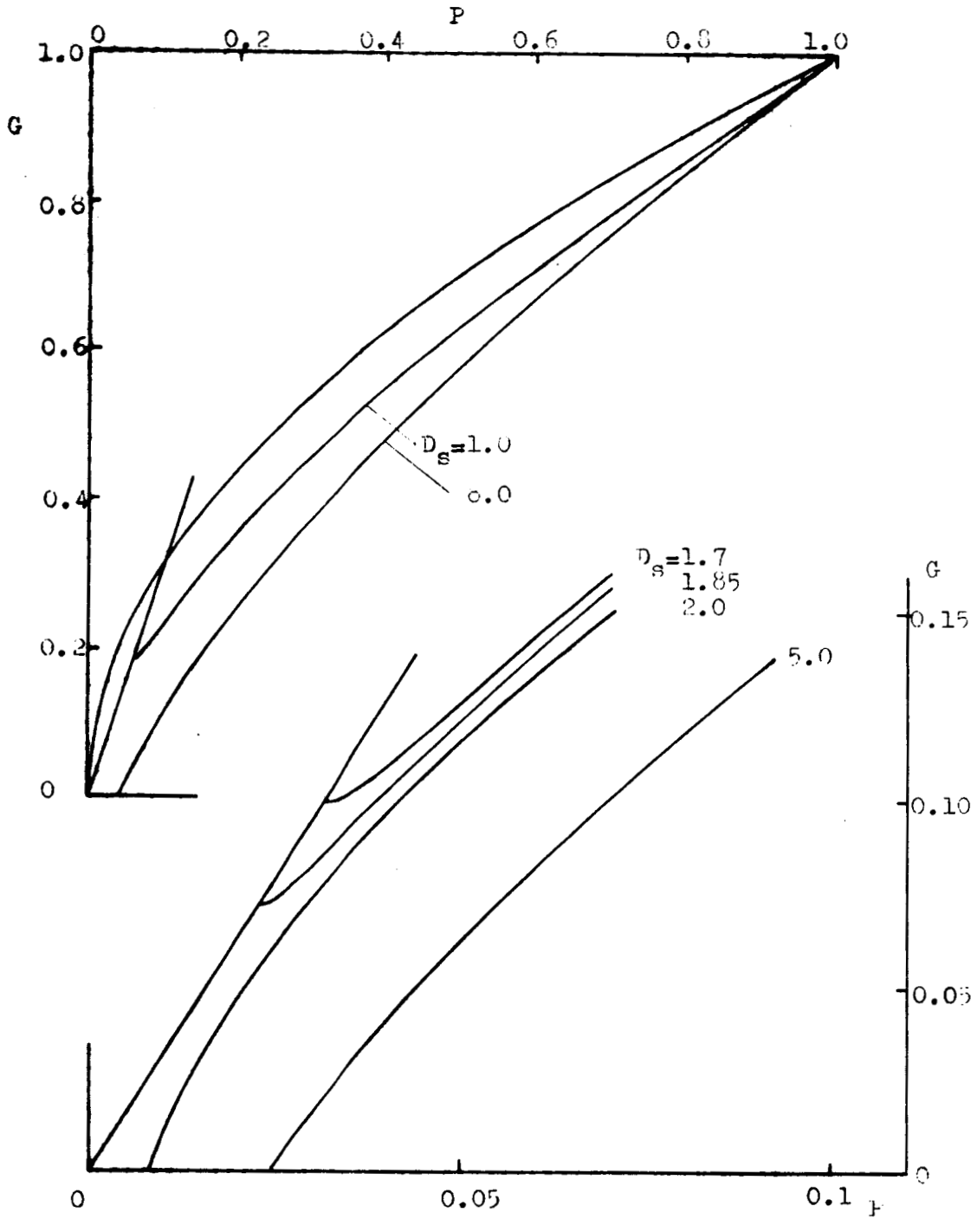

Figure 5. Variation of burning rate with pressure during depressurization at various depressurization rates. The upper part of the figure shows the gross effect. The lower part is a detailed view of the lower left hand corner. The straight line originating at the origins is the mass flux through the expanded nozzle. n = 1.0, E = 5.56, Δh_w = 0, P_2/P_1 = 0.1.

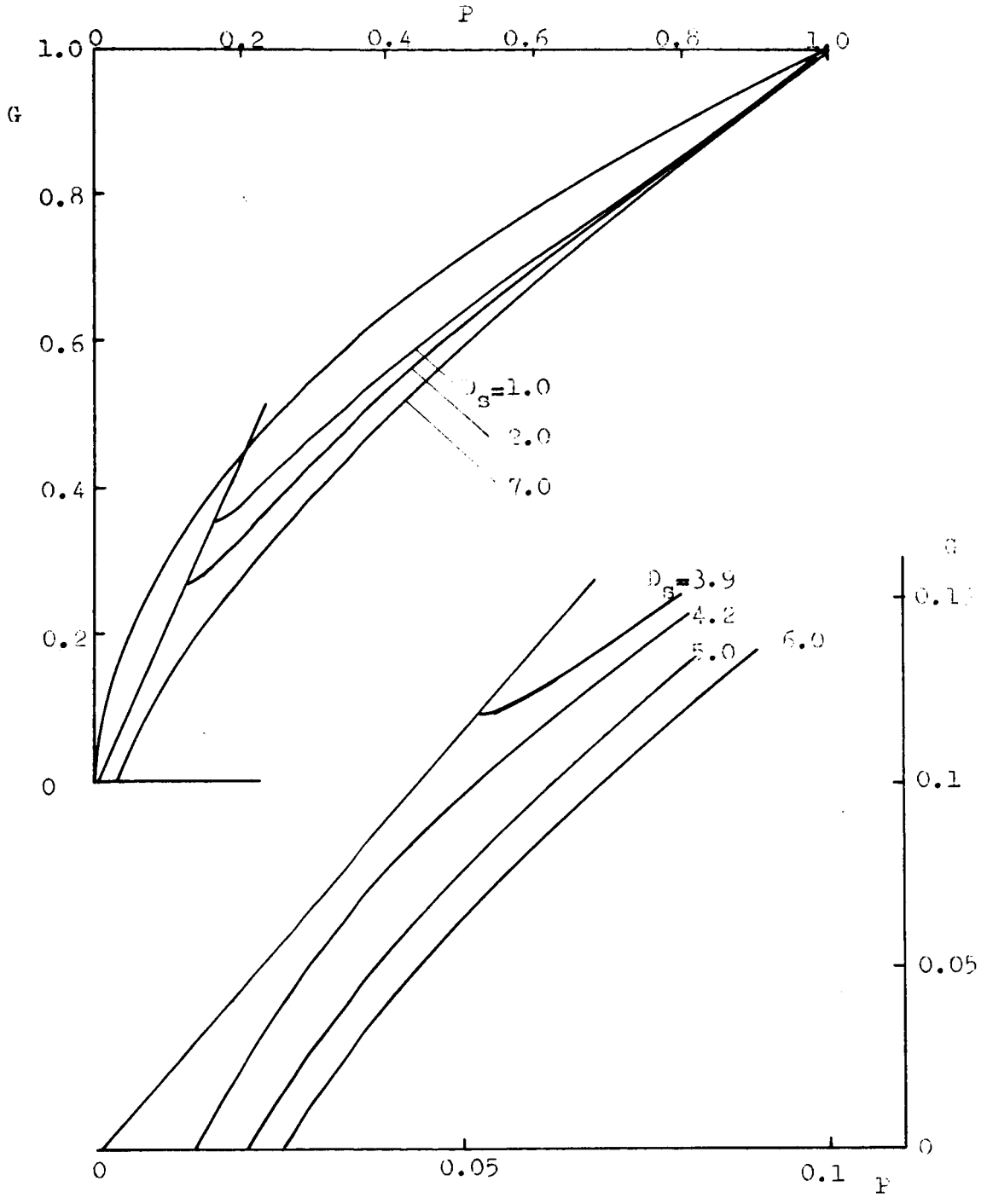

Figure 6. Variation of burning rate with pressure during depressurization at various depressurization rates. The upper part of the figure shows the gross effect. The lower part is a detailed view of the lower left hand corner. The straight line originating at the origins is the mass flux through the expanded nozzle. n = 1.0, E - 5.56, Δh_w = 0, P_2/P_1 = 0.2.

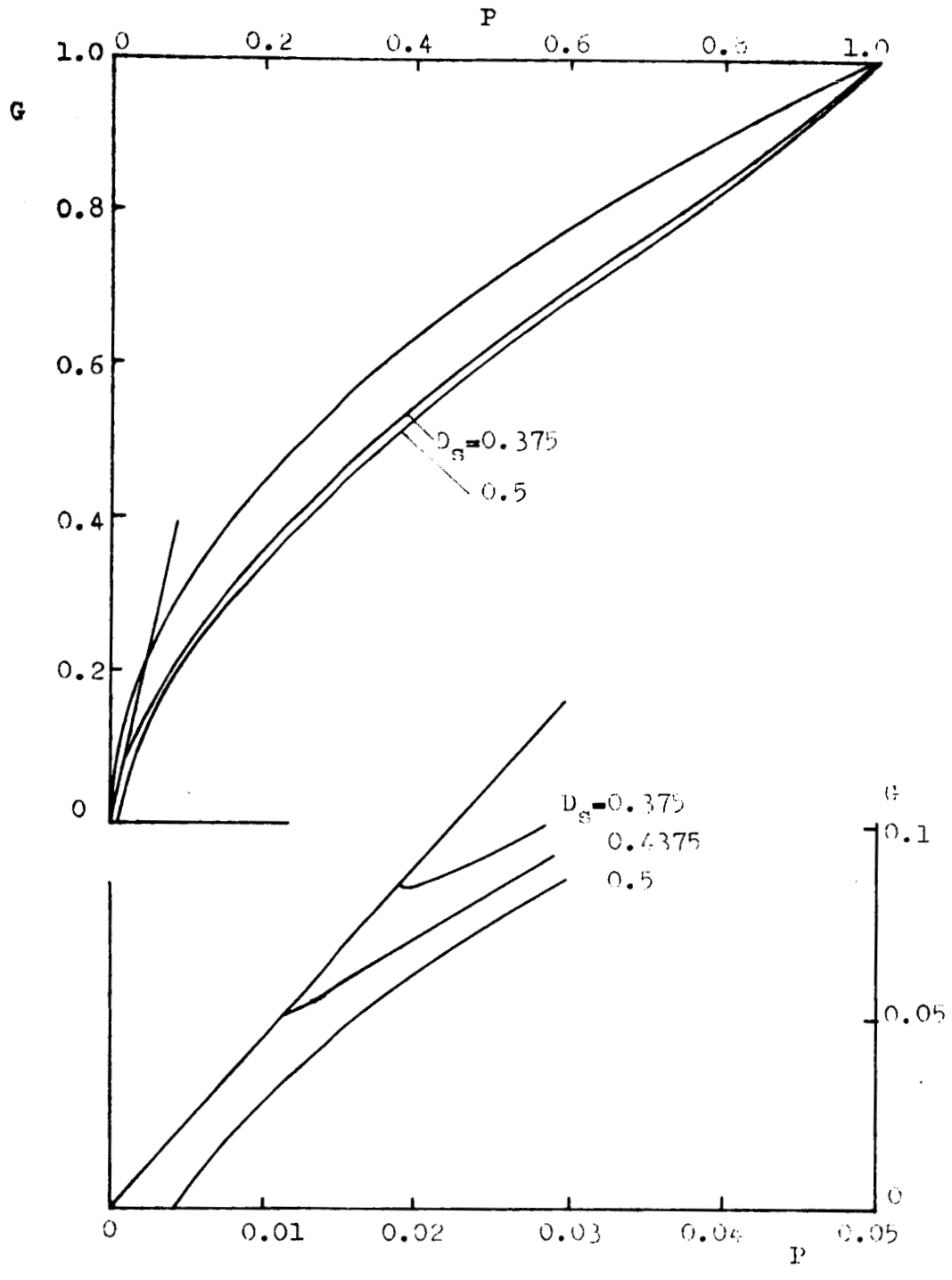

Figure 7. Variation of burning rate with pressure during depressurization at various depressurization rates. The upper part of the figure shows the gross effect. The lower part is a detailed view of the lower left hand corner. The straight line originating at the origins is the mass flux through the expanded nozzle. n = 1, E = 5.56, Δh_w = -0.2, P_2/P_1 = 0.05.

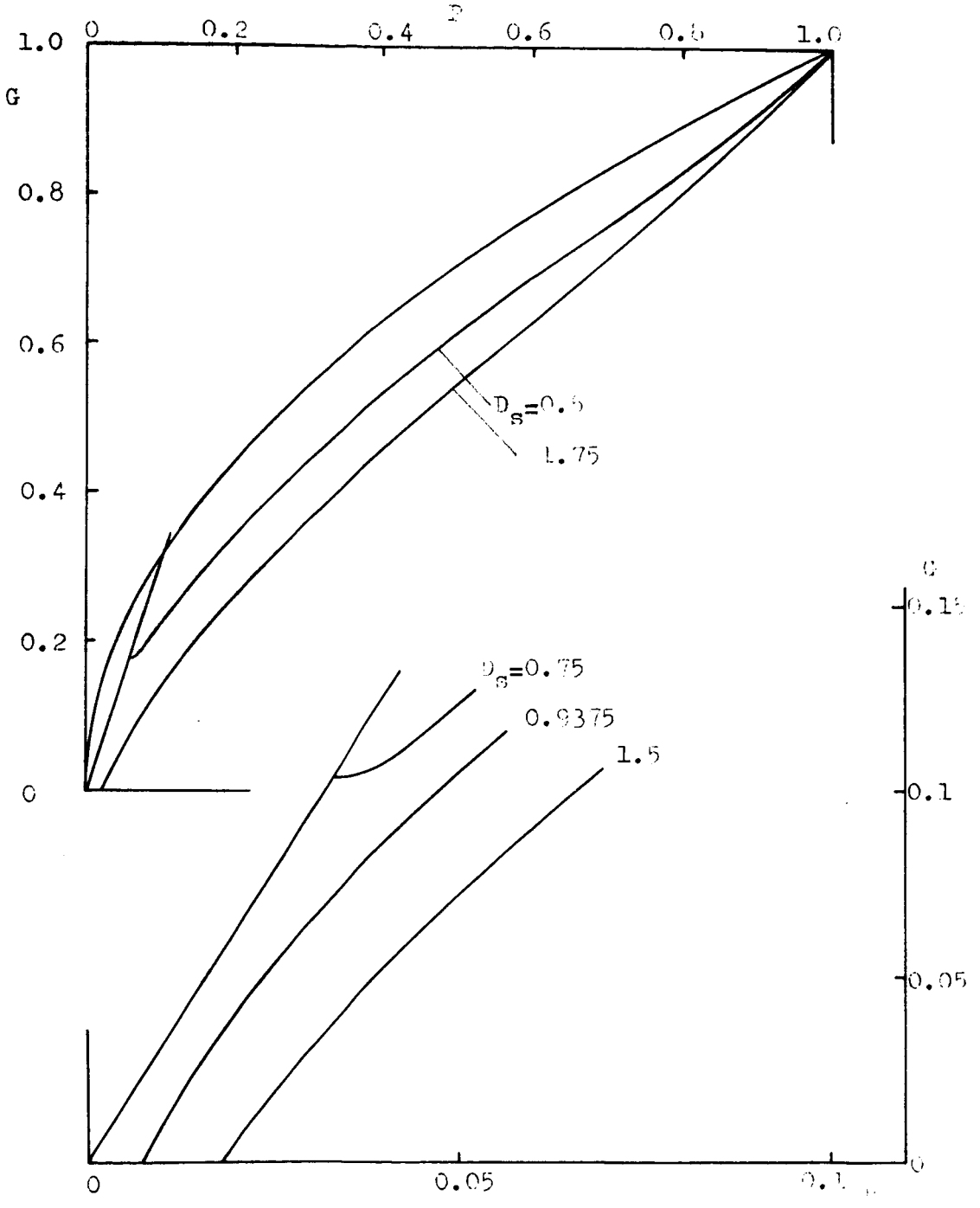

Figure 8. Variation of burning rate with pressure during depressurization at various depressurization rates. The upper part of the figure shows the gross effect. The lower part is a detailed view of the lower left hand corner. The straight line originating at the origins is the mass flux through the expanded nozzle. n = 1.0, E = 5.56, Δh_w = -0.2, P P_2/P_1 = 0.1

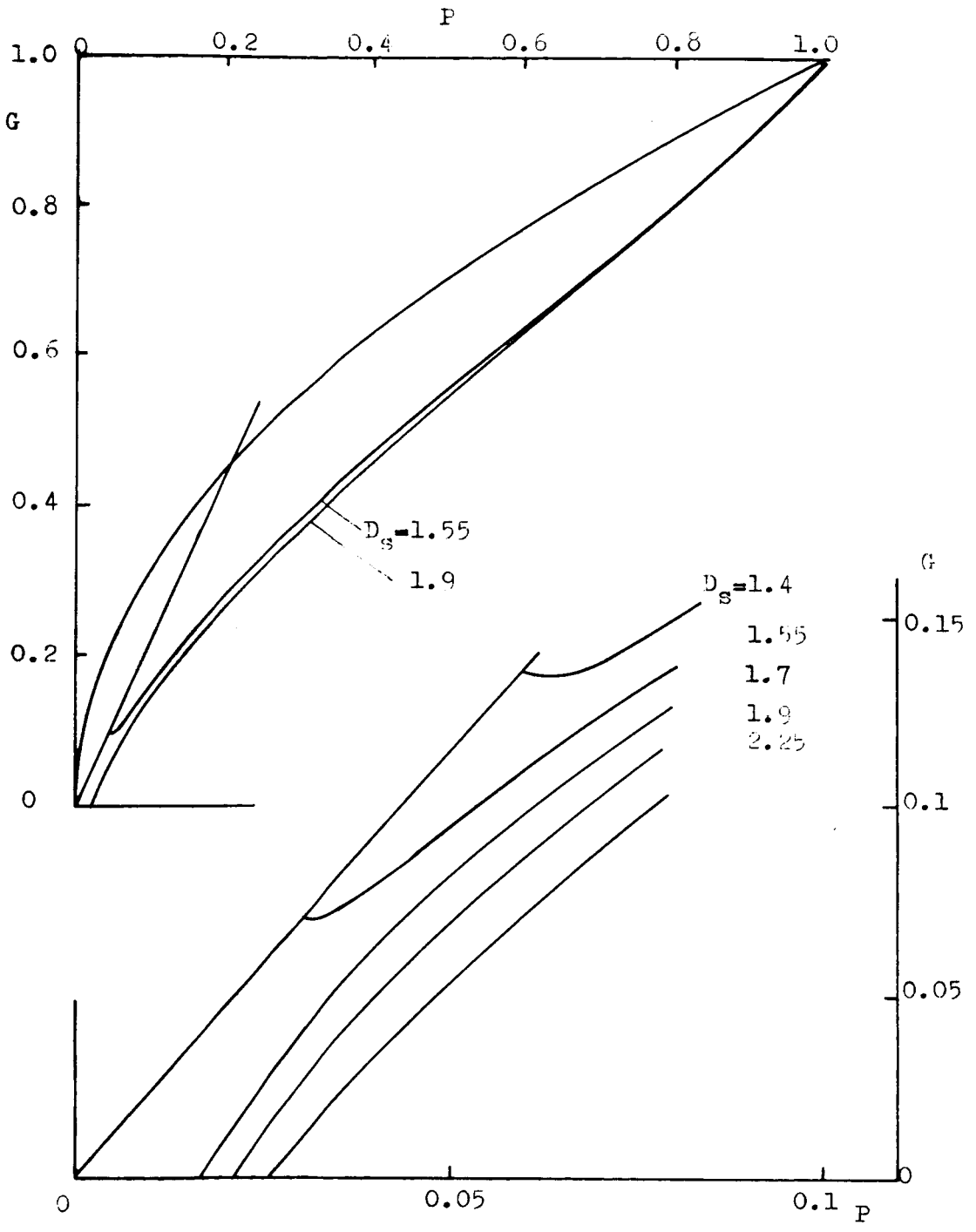

Figure 9. Variations of burning rate with pressure during depressurization at various depressurization rates. The upper part of the figure shows the gross effect. The lower part is a detailed view of the lower left hand corner. The straight line originating at the origins is the mass flux through the expanded nozzle. n = 1.0, E = 5.56, Δh_w = -0.2, P_2/P_1 = 0.2.

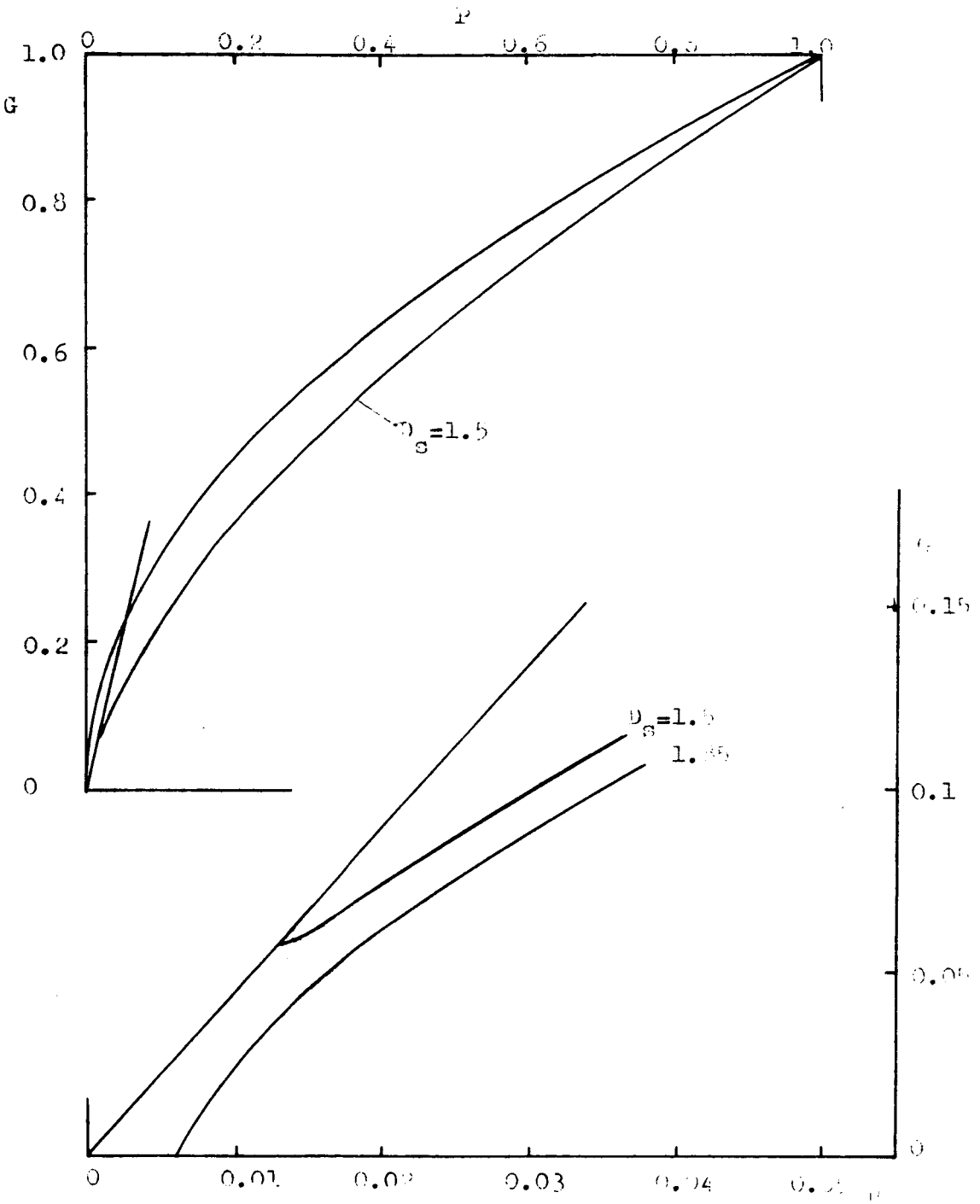

Figure 10. Variations of burning rate with pressure during depressurization at various depressurization rates. The upper part of the figure shows the gross effect. The lower part is a detailed view of the lower left hand corner. The straight line originating at the origins is the mass flux through the expanded nozzle. $n = 1.0$, $E = 5.56$, $\Lambda h_w = 0.2$, $P_2/P_1 = 0.05$.

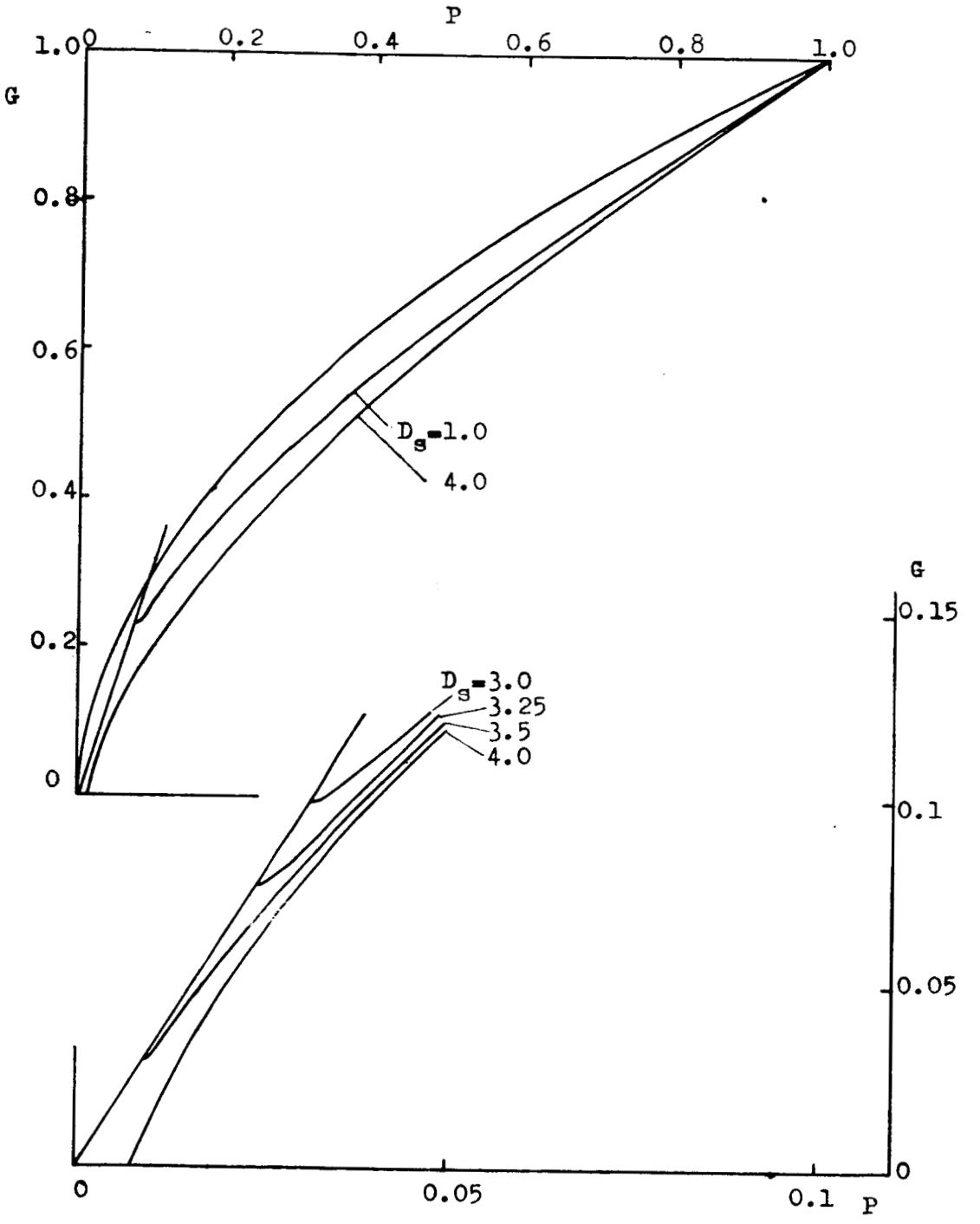

Figure 11. Variations of burning rate with pressure during depressurization at various depressurization rates. The upper part of the figure shows the gross effect. The lower part is a detailed view of the lower left hand corner. The straight line originating at the origins is the mass flux through the expanded nozzle. $n = 1.0$, $E = 5.56$, $\Lambda h_w = 0.2$, $P_2/P_1 = 0.1$.

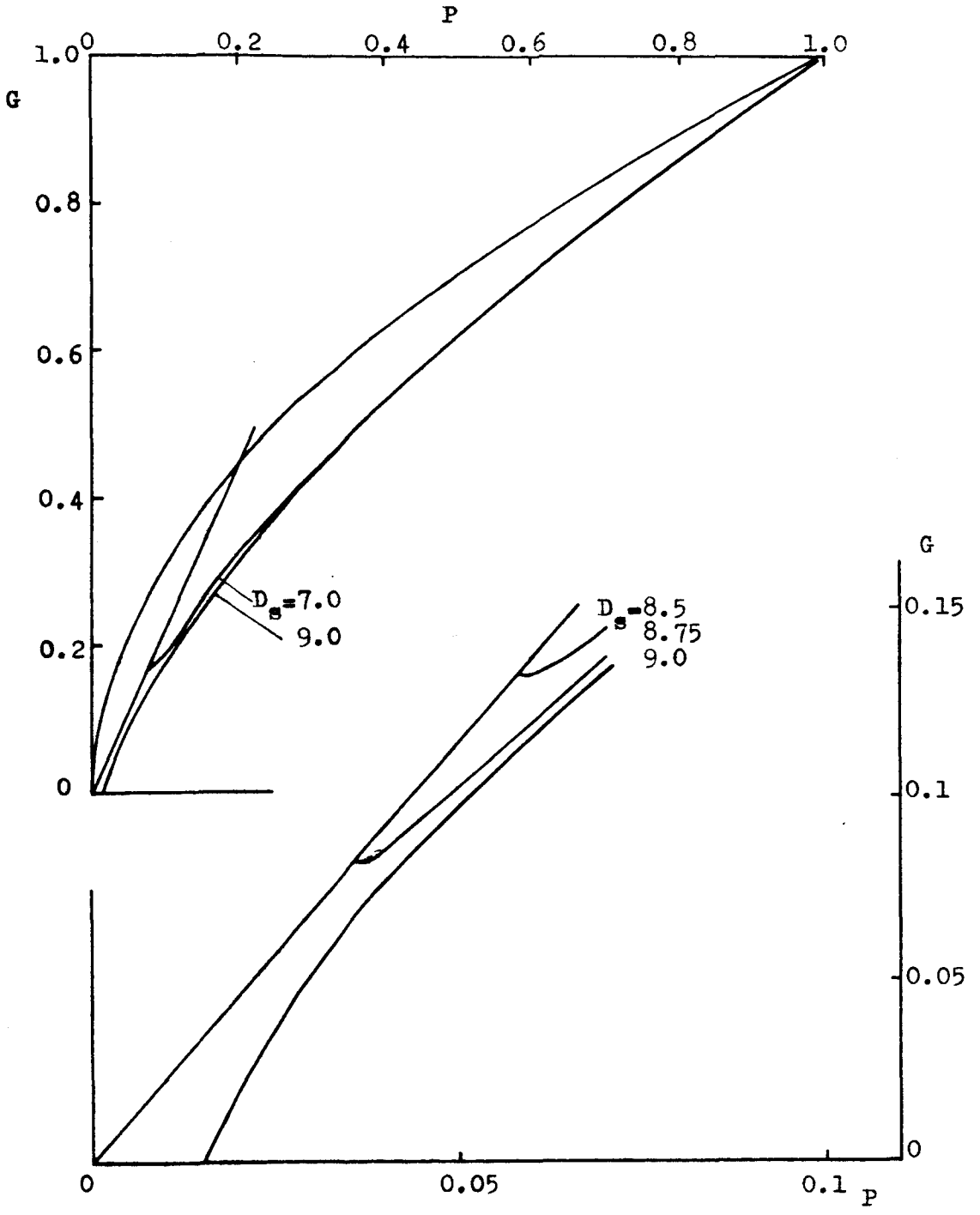

Figure 12. Variations of burning rate with pressure during depressurization at various depressurization rates. The upper part of the figure shows the gross effect. The lower part is a detailed view of the lower left hand corner. The straight line originating at the origins is the mass flux through the expanded nozzle. $n = 1.0$, $\bar{E} = 5.56$, $\Delta h_w = 0.2$, $P_2/P_1 = 0.2$.

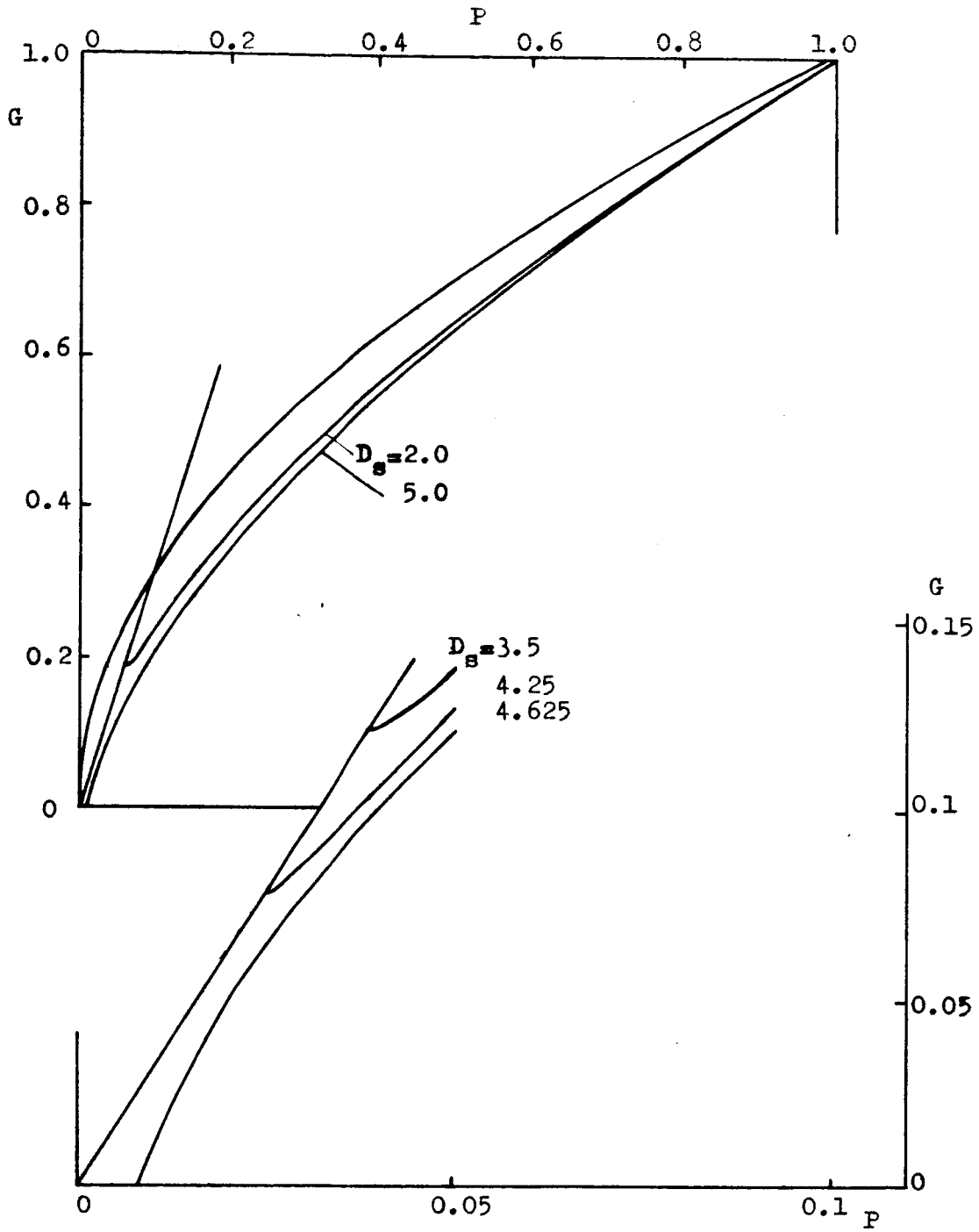

Figure 13. Variations of burning rate with pressure during depressurization at various depressurization rates. The upper part of the figure shows the gross effect. The lower part is a detailed view of the lower left hand corner. The straight line originating at the origins is the mass flux through the expanded nozzle. $n = 1.0$, $E = 11.12$, $\Delta h_w = 0$, $P_2/P_1 = 0.1$.

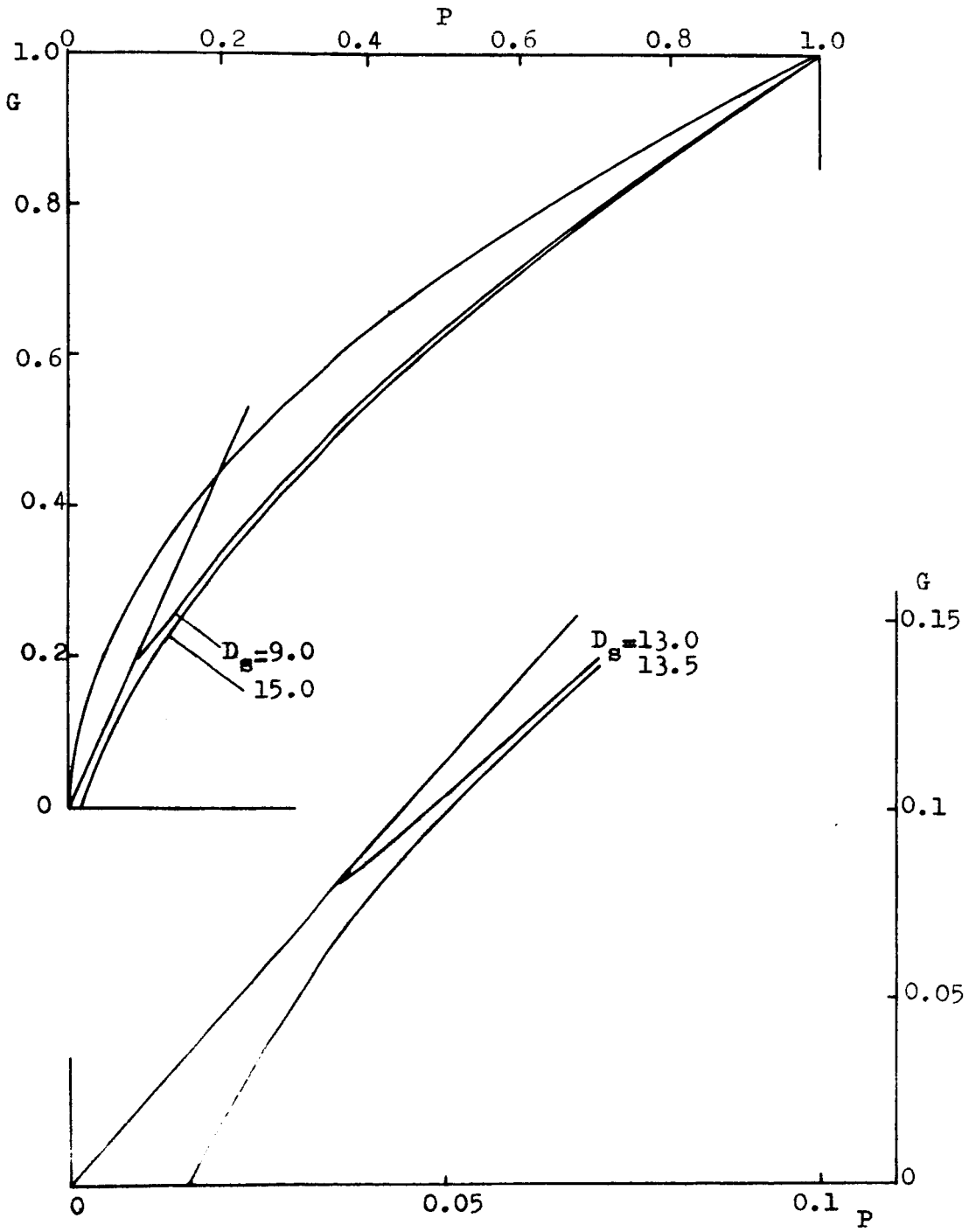

Figure 14. Variations of burning rate with pressure during depressurization at various depressurization rates. The upper part of the figure shows the gross effect. The lower part is a detailed view of the lower left hand corner. The straight line originating at the origins is the mass flux through the expanded nozzle. $n = 1.0$, $E = 11.12$, $\Delta h_w = 0$, $P_2/P_1 = 0.2$.

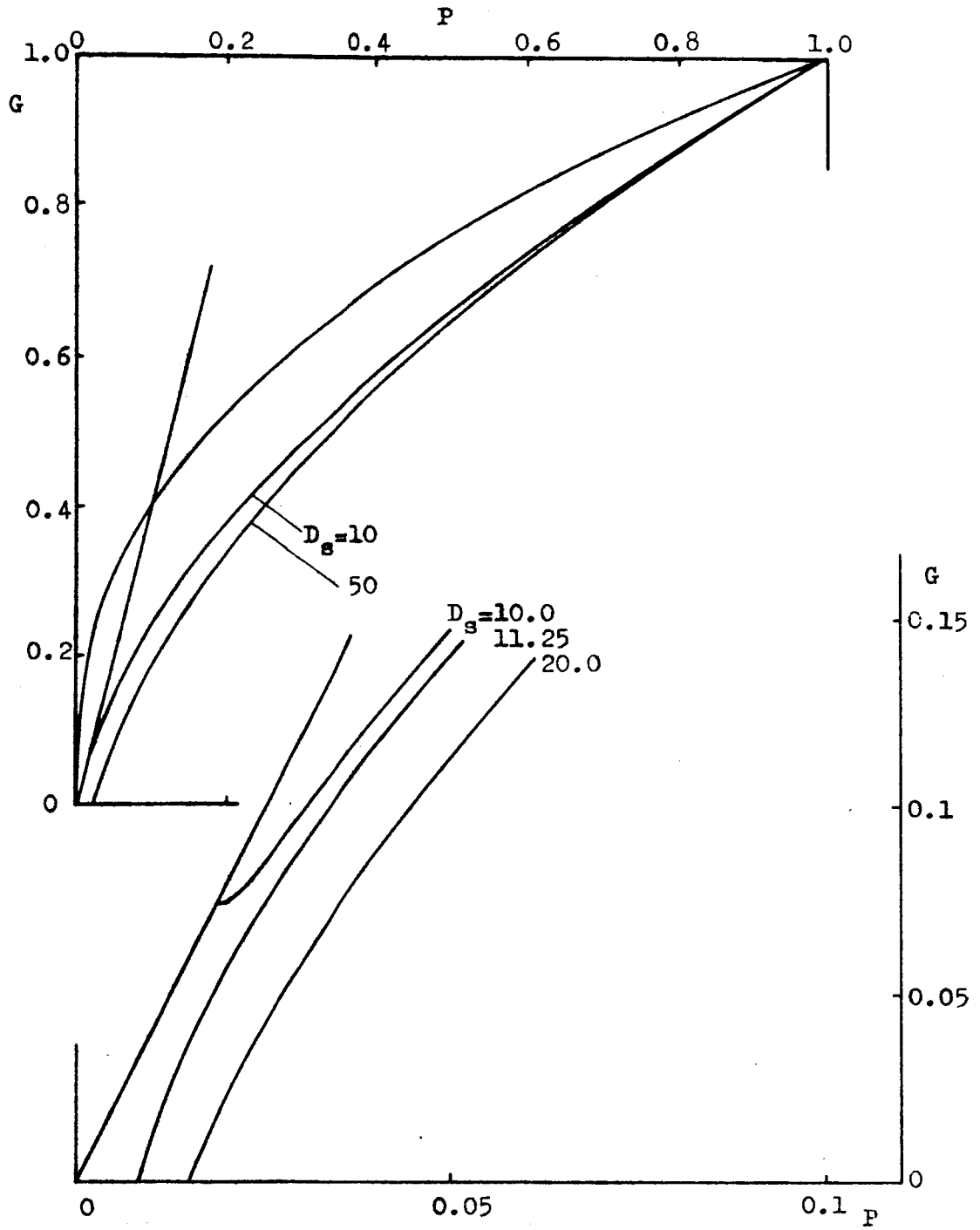

Figure 15. Variations of burning rate with pressure during depressurization at various depressurization rates. The upper part of the figure shows the gross effect. The lower part is a detailed view of the lower left hand corner. The straight line originating at the origins is the mass flux through the expanded nozzle. $n = 0.8$, $E = 5.56$, $\Delta h_w = 0$, $P_2/P_1 = 0.1$.

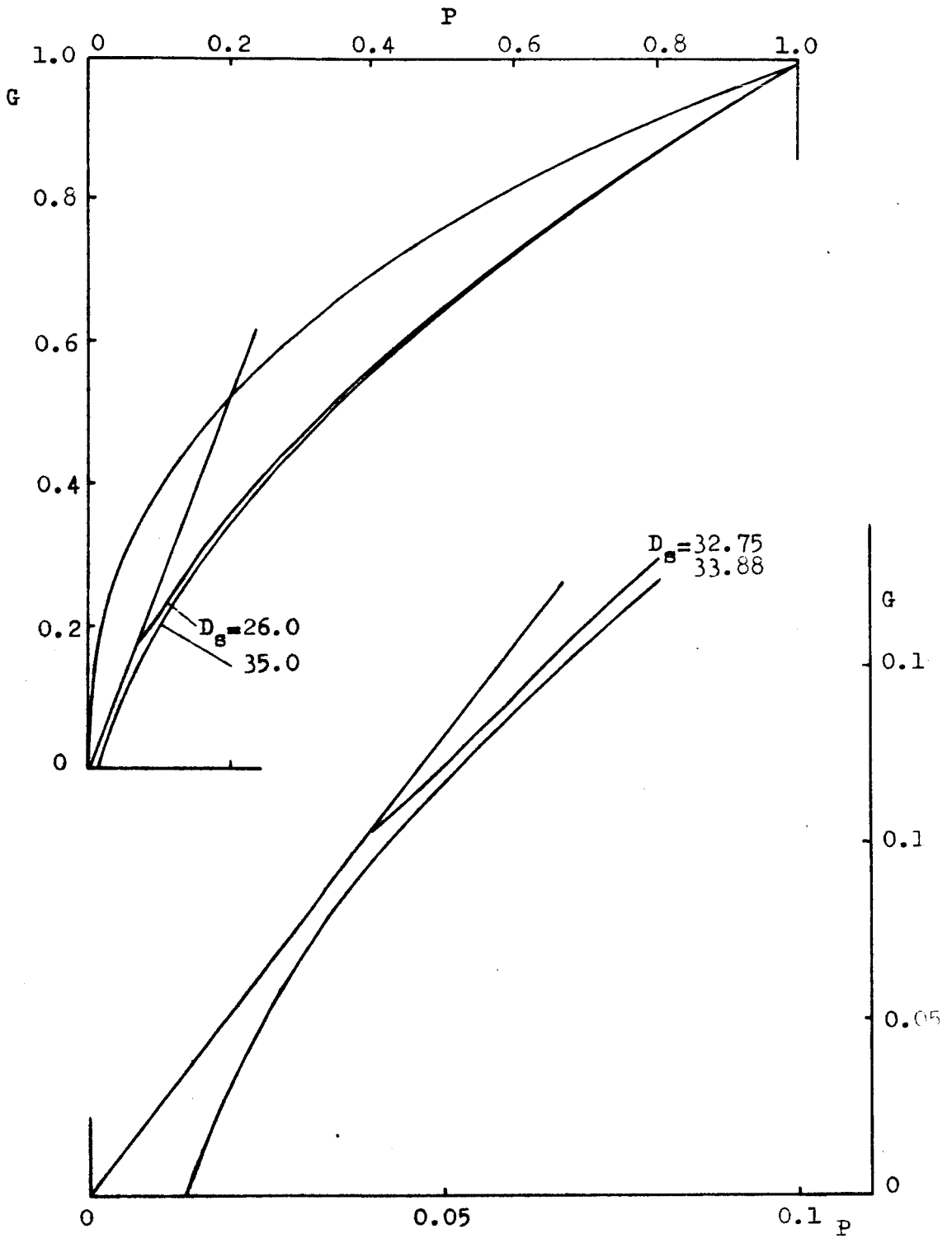

Figure 16. Variations of burning rate with pressure during depressurization at various depressurization rates. The upper part of the figure shows the gross effect. The lower part is a detailed view of the lower left hand corner. The straight line originating at the origins is the mass flux through the expanded nozzle. n = 0.8, E = 5.56, $\Delta h_w = 0$, $P_2/P_1 = 0.2$.

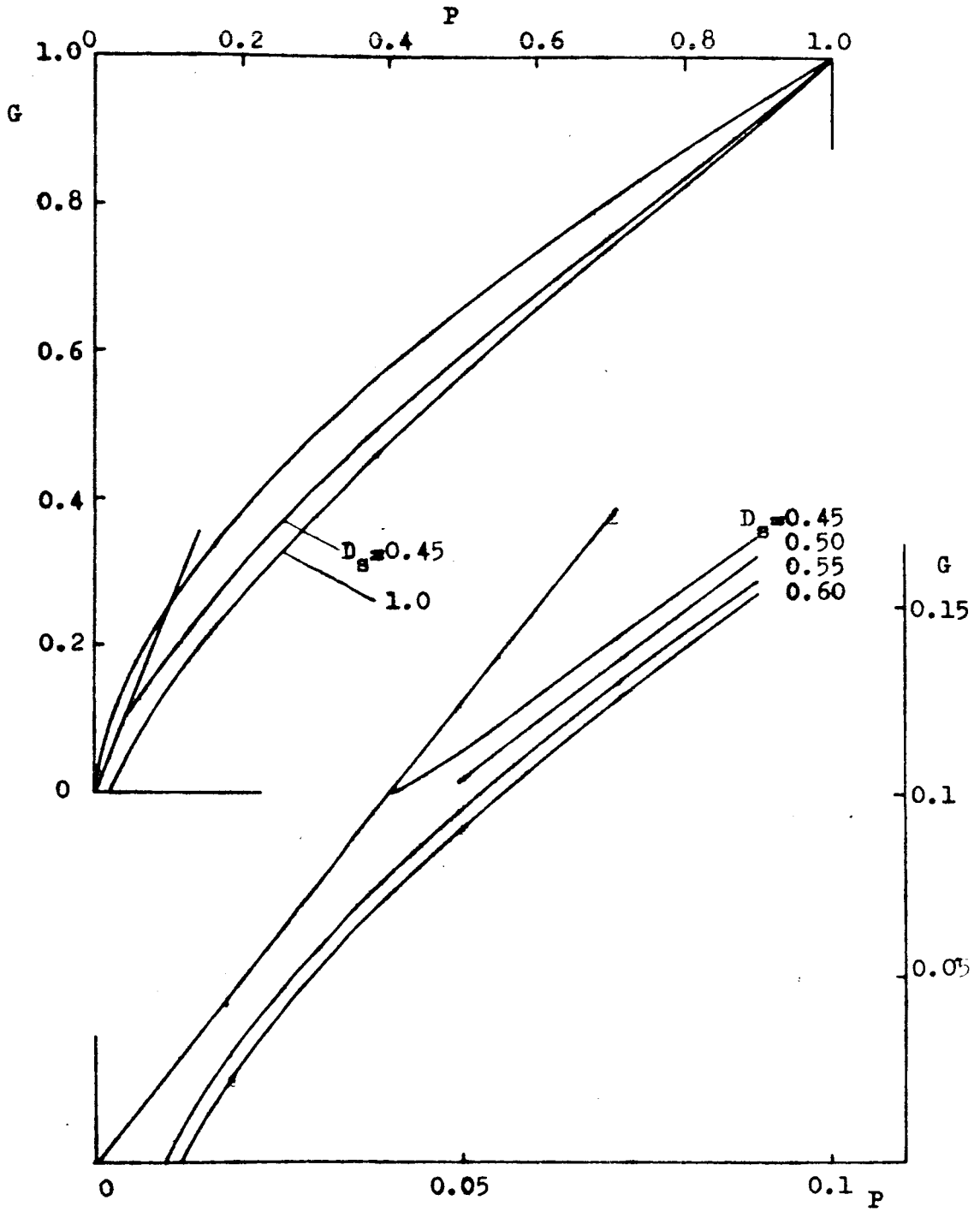

Figure 17. Variations of burning rate with pressure during depressurization at various depressurization rates. The upper part of the figure shows the gross effect. The lower part is a detailed view of the lower left hand corner. The straight line originating at the origins is the mass flux through the expanded nozzle. $n = 1.2$, $E = 5.56$, $\Delta h_w = 0$, $P_2/P_1 = 0.1$.

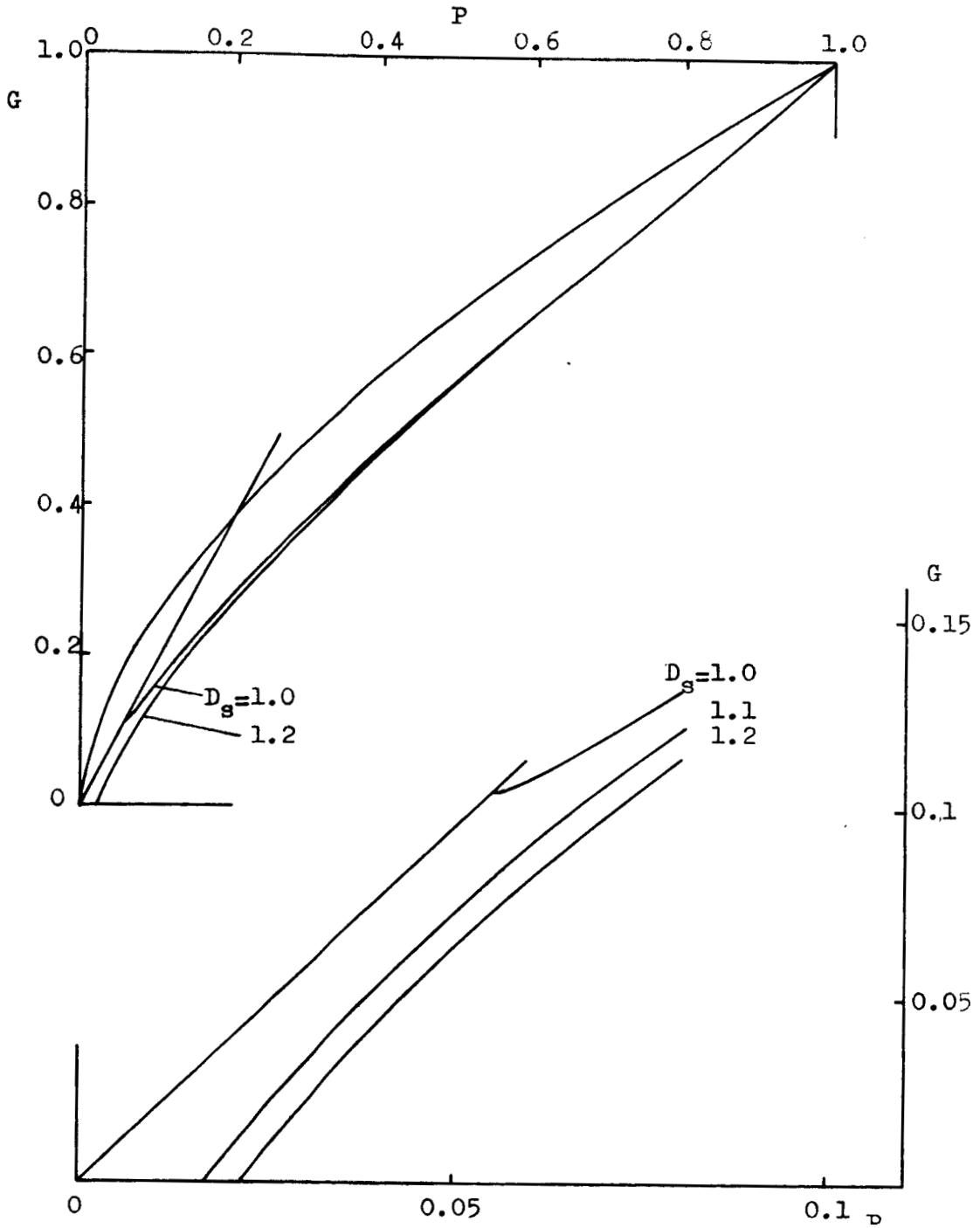

Figure 18. Variations of burning rate with pressure during depressurization at various depressurization rates. The upper part of the figure shows the gross effect. The lower part is a detailed view of the lower left hand corner. The straight line originating at the origins is the mass flux through the expanded nozzle. $n = 1.2$, $E = 5.56$, $\Delta h_w = 0$, $P_2/P_1 = 0.2$.

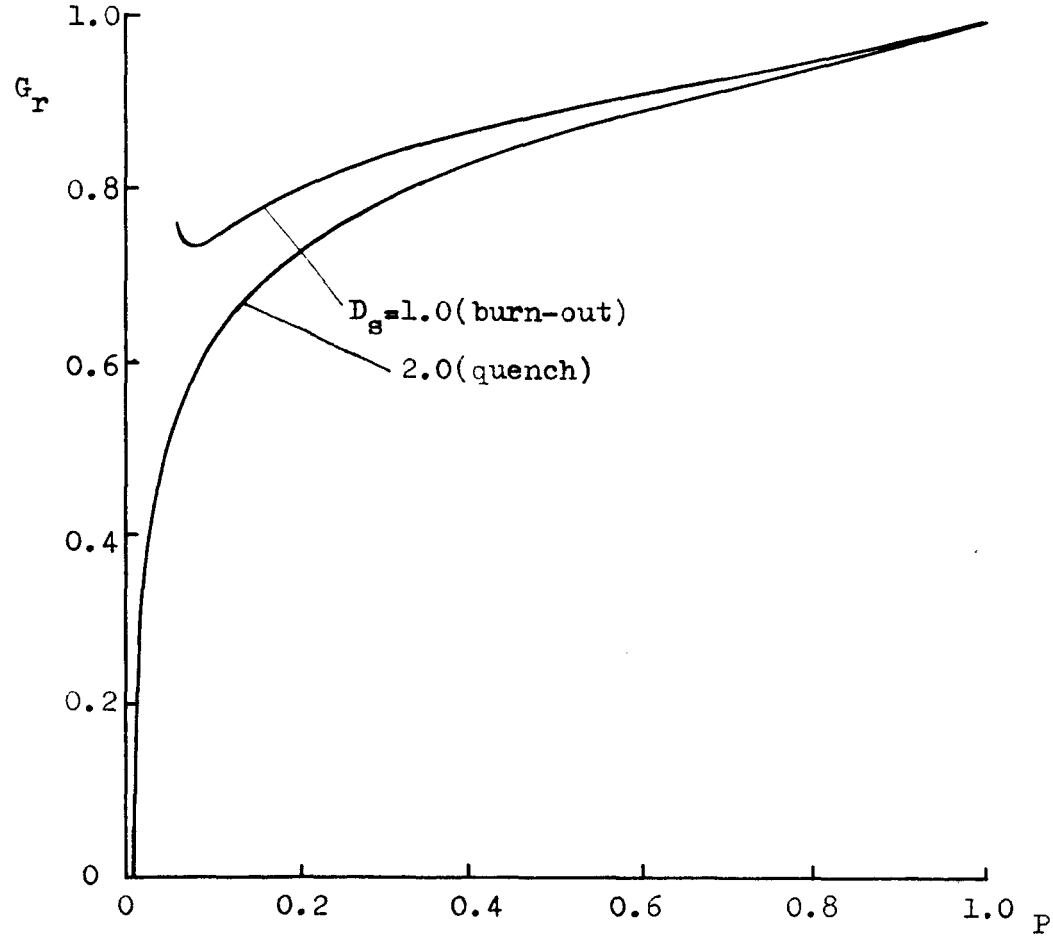

Figure 19. Variation of burning rate with pressure during depressurization for the case: n = 1, E = 5.56, $\Delta h_w = 0$, and $P_2/P_1 = 0.1$. The curves show how the differences between burning rates become more pronounced as depressurization proceeds.

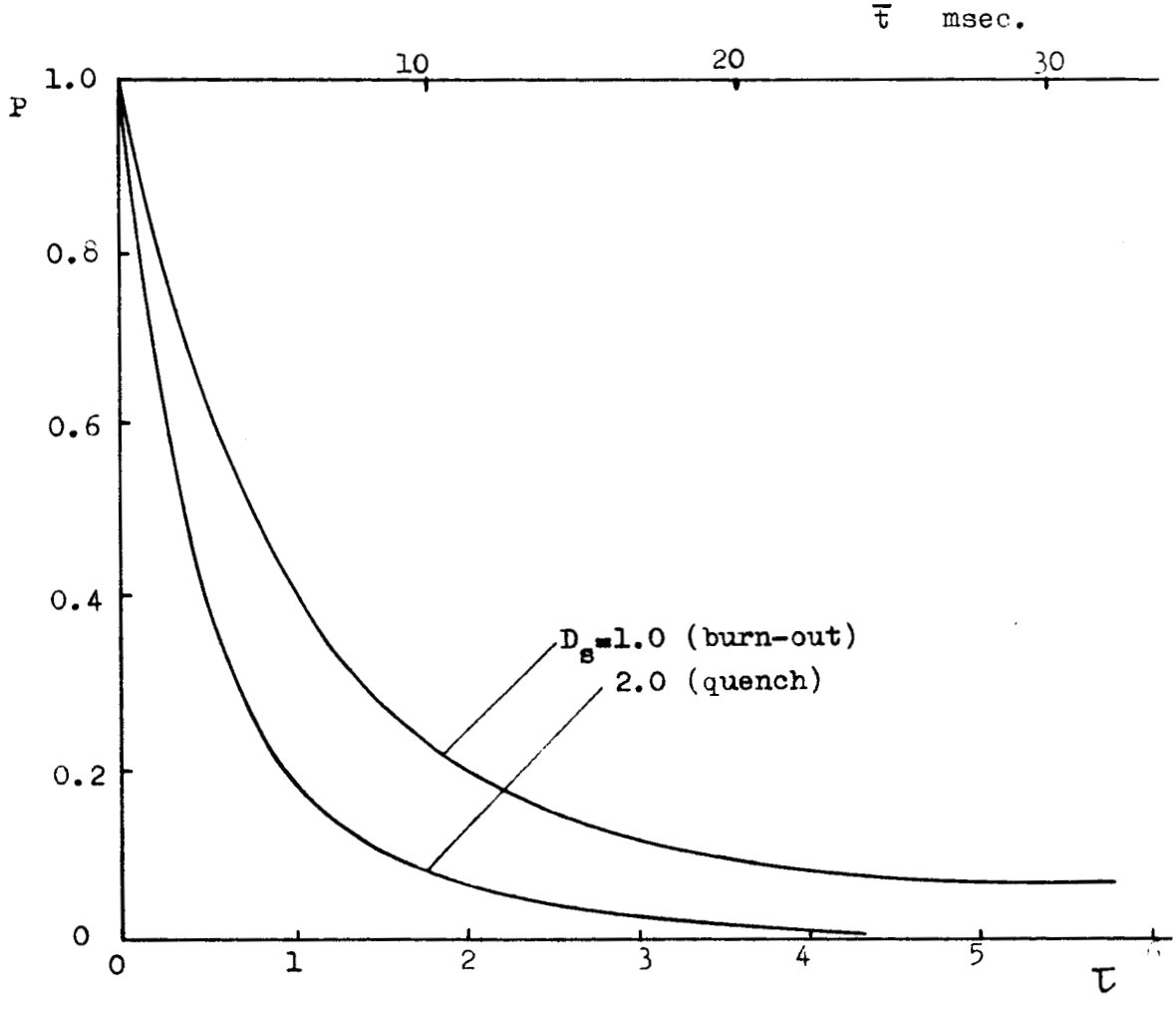

Figure 20. Variation of chamber pressure with time for two different pressurization rates; n = 1, E = 5.56, $\Lambda h_w = 0$, $P_2/P_1 = 0.1$.

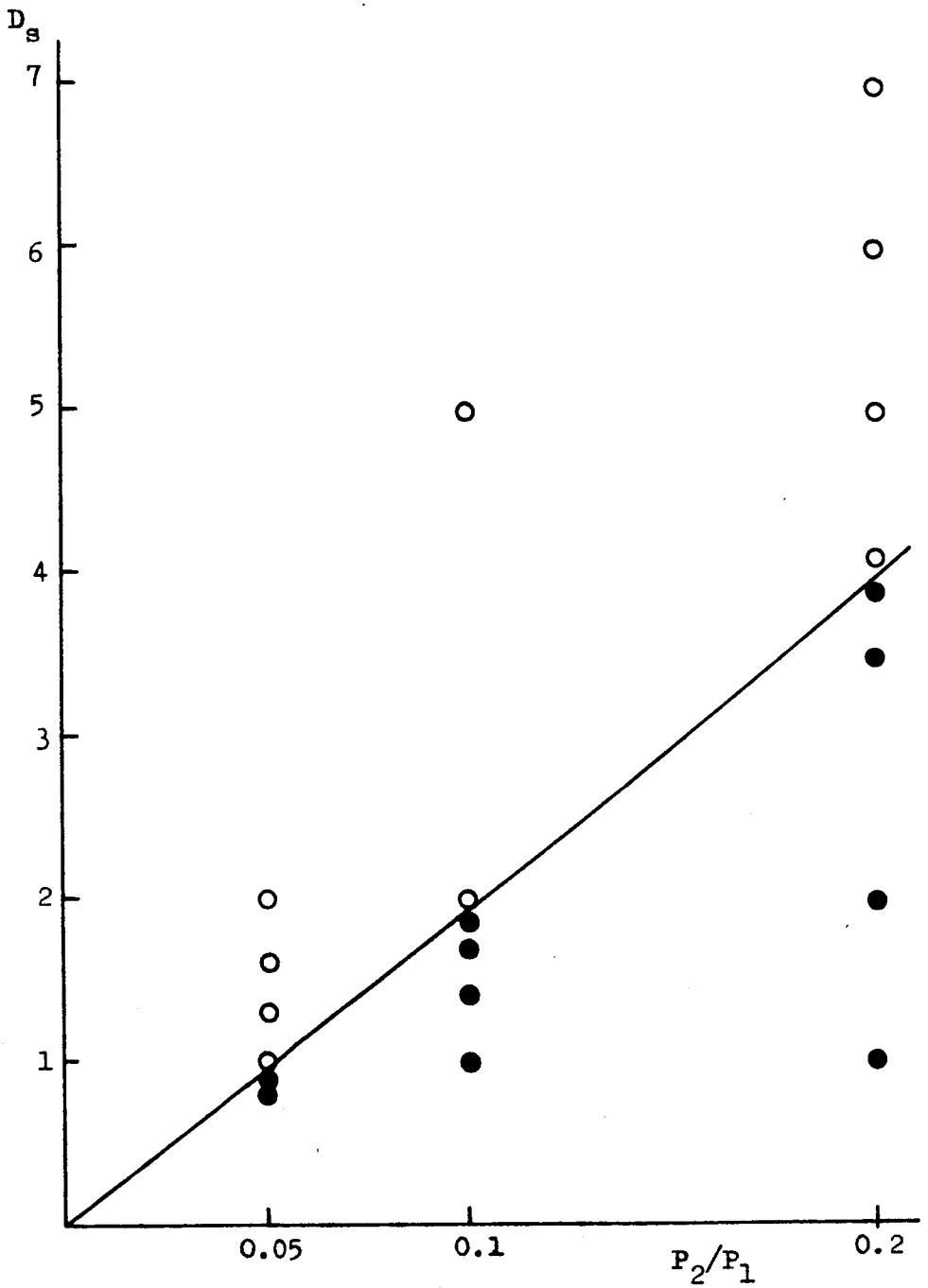

Figure 21. Quench limit obtained in computer experiments. The open symbols represent experiments in which the propellant quenched. The solid symbols represent experiments in which the propellant continued to burn. $n = 1.0$, $E = 5.56$, and $\Delta h_w = 0$.

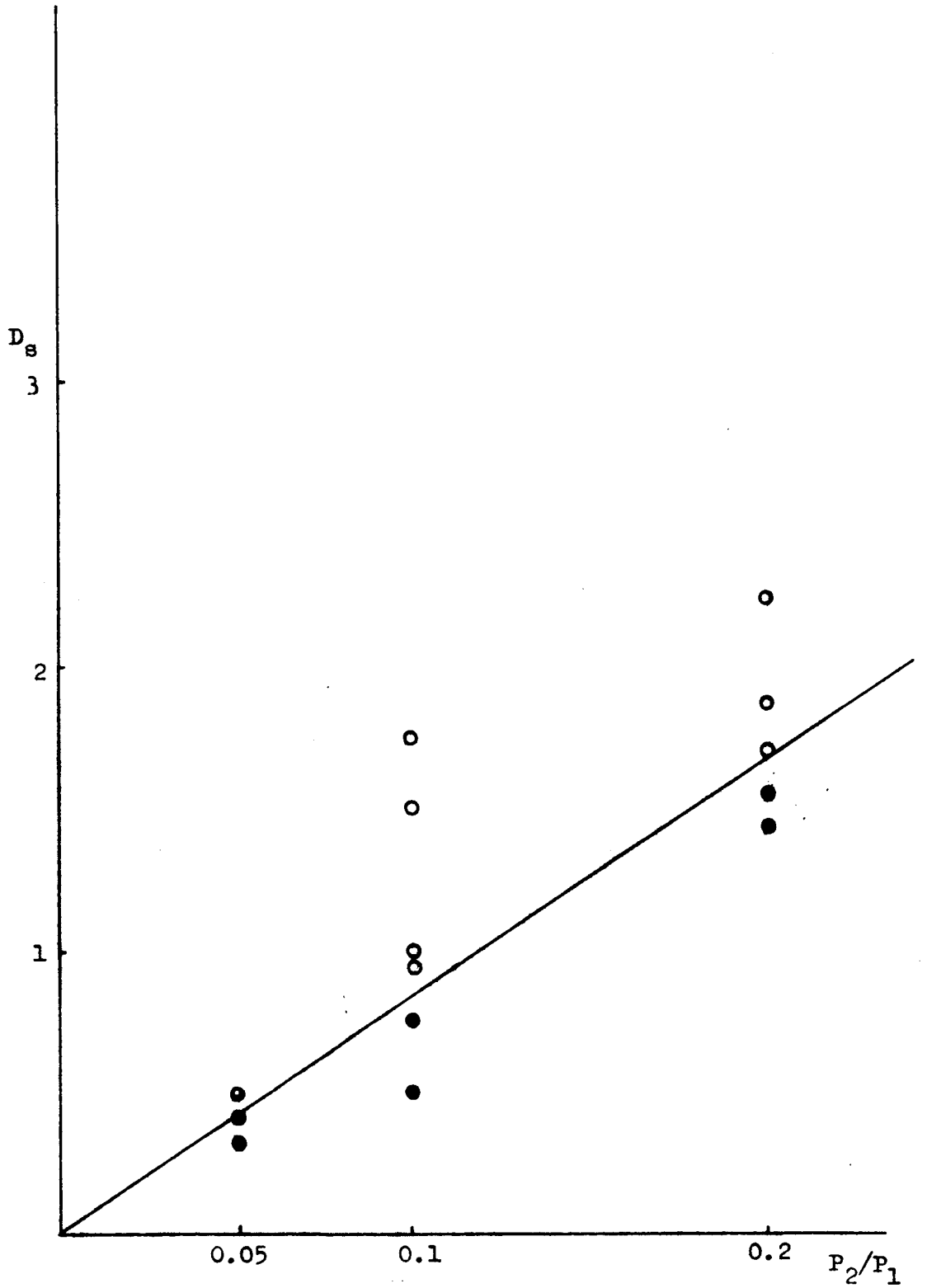

Figure 22. Quench limit obtained in computer experiments. The open symbols represent experiments in which the propellant quenched. The solid symbols represent experiments in which the propellant continued to burn. $n = 1.0$, $E = 5.56$, $\Delta h_w = -0.2$.

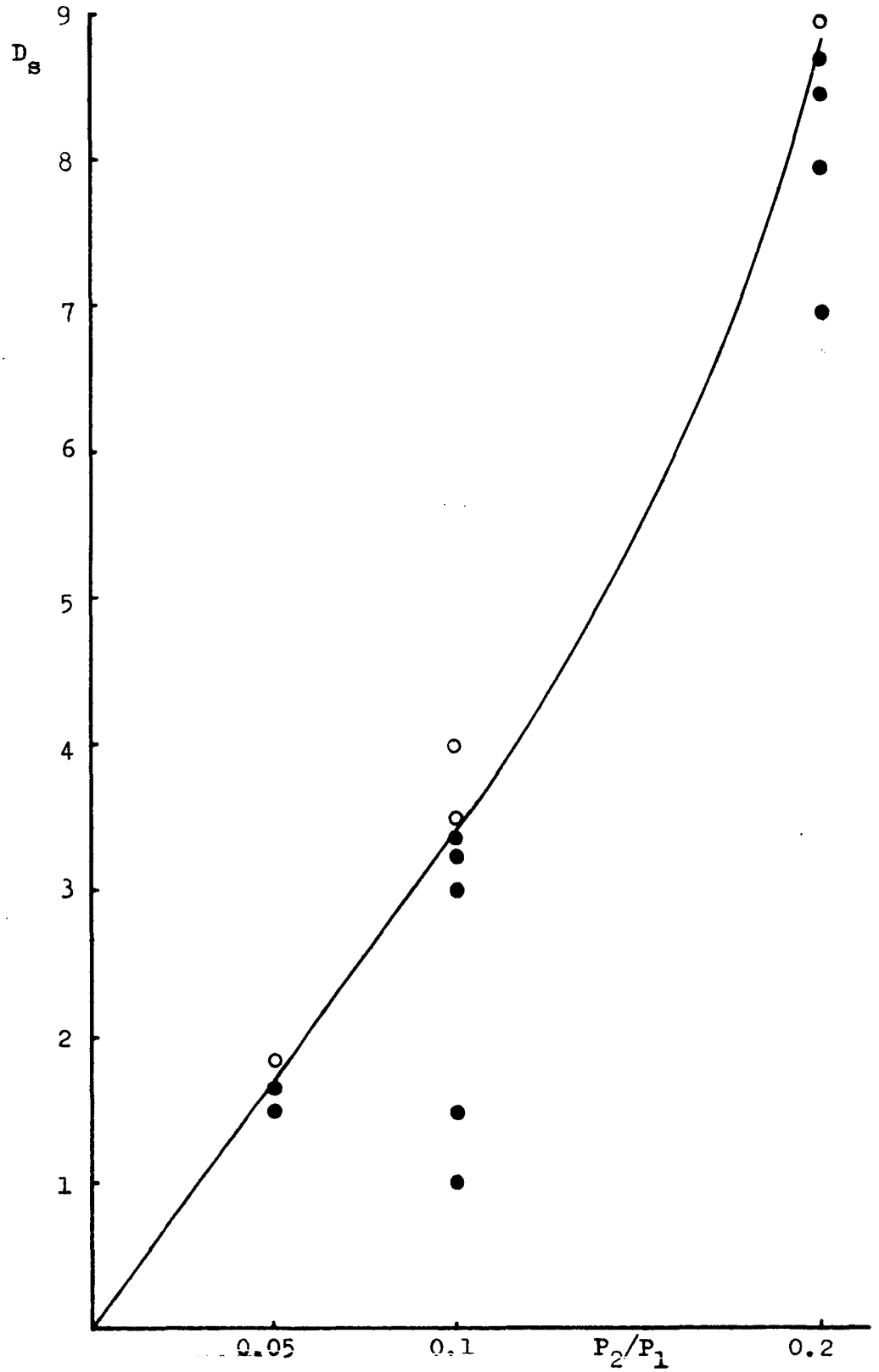

Figure 23. Quench limit obtained in computer experiments. The open symbols represent experiments in which the propellant quenched. The solid symbols represent experiments in which the propellant continued to burn. $n = 1.0$, $E = 5.56$, $\Lambda h_w = 0.2$.

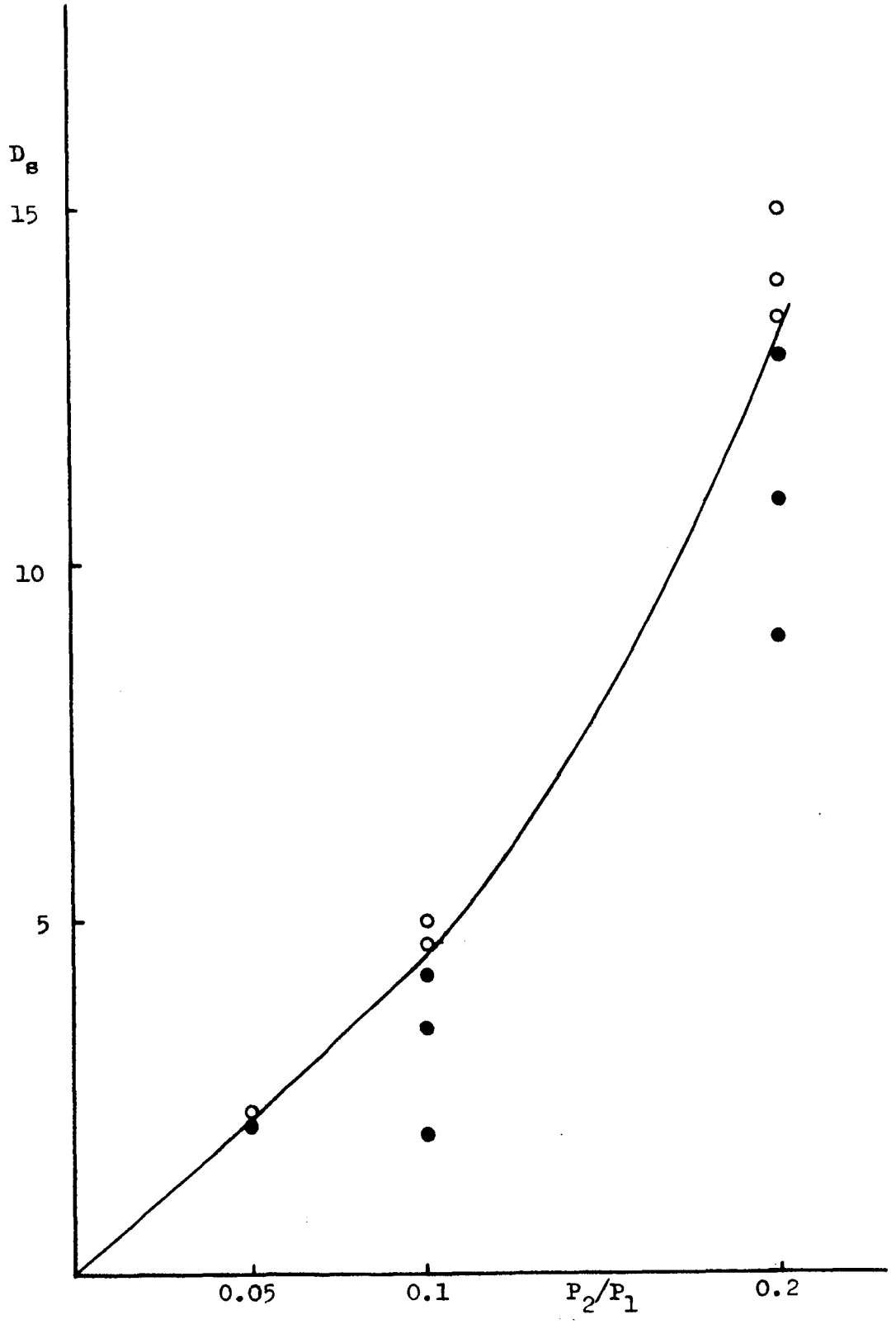

Figure 24. Quench limit obtained in computer experiments. The open symbols represent experiments in which the propellant quenched. The solid symbols represent experiments in which the propellant continued to burn. $n = 1.0$, $E = 11.12$, $\Delta h_w = 0$.

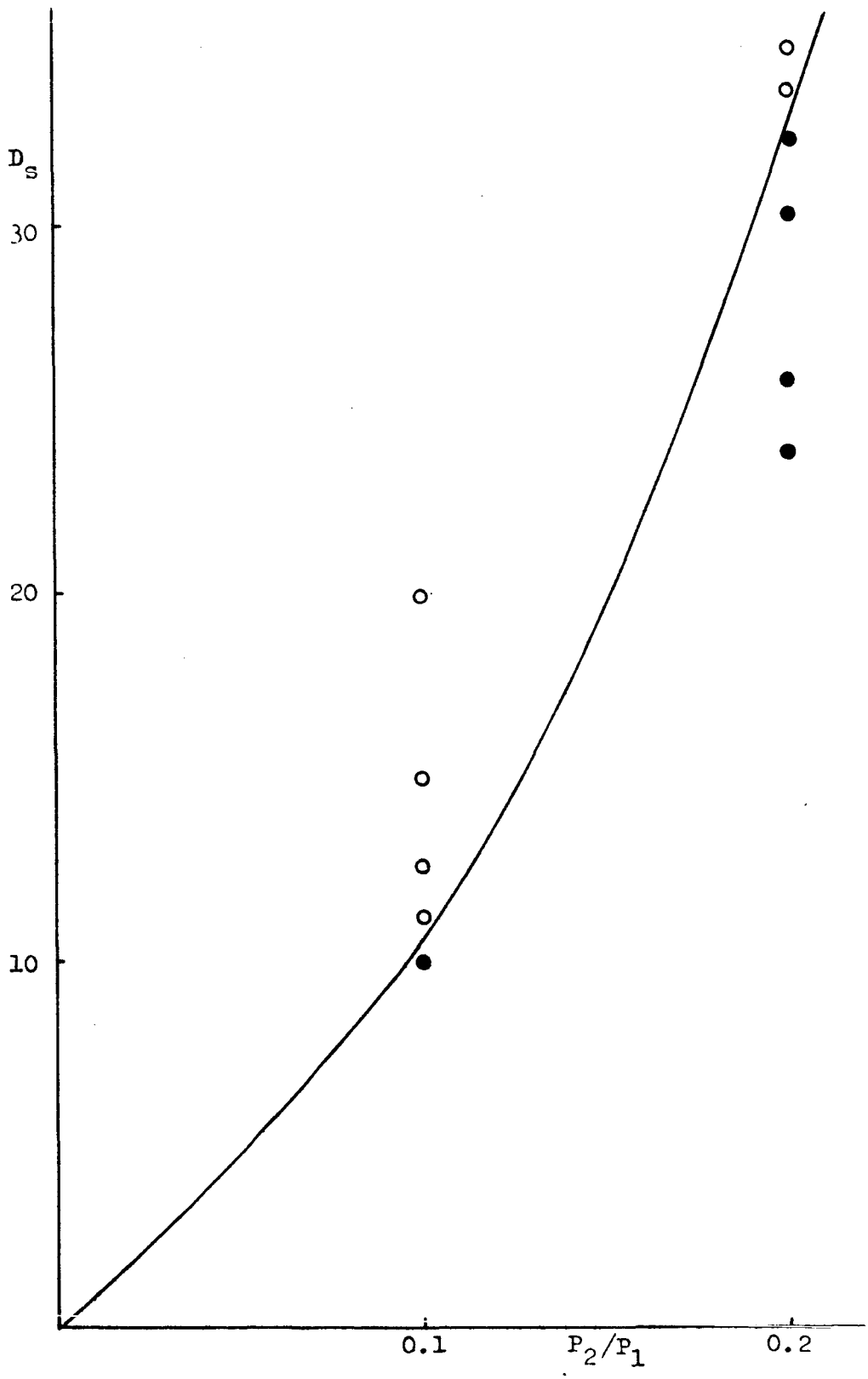

Figure 25. Quench limit obtained in computer experiments. The open symbols represent experiments in which the propellant quenched. The solid symbols represent experiments in which the propellant continued to burn. $n = 0.8$, $E = 5.56$, $\Delta h_w = 0$.

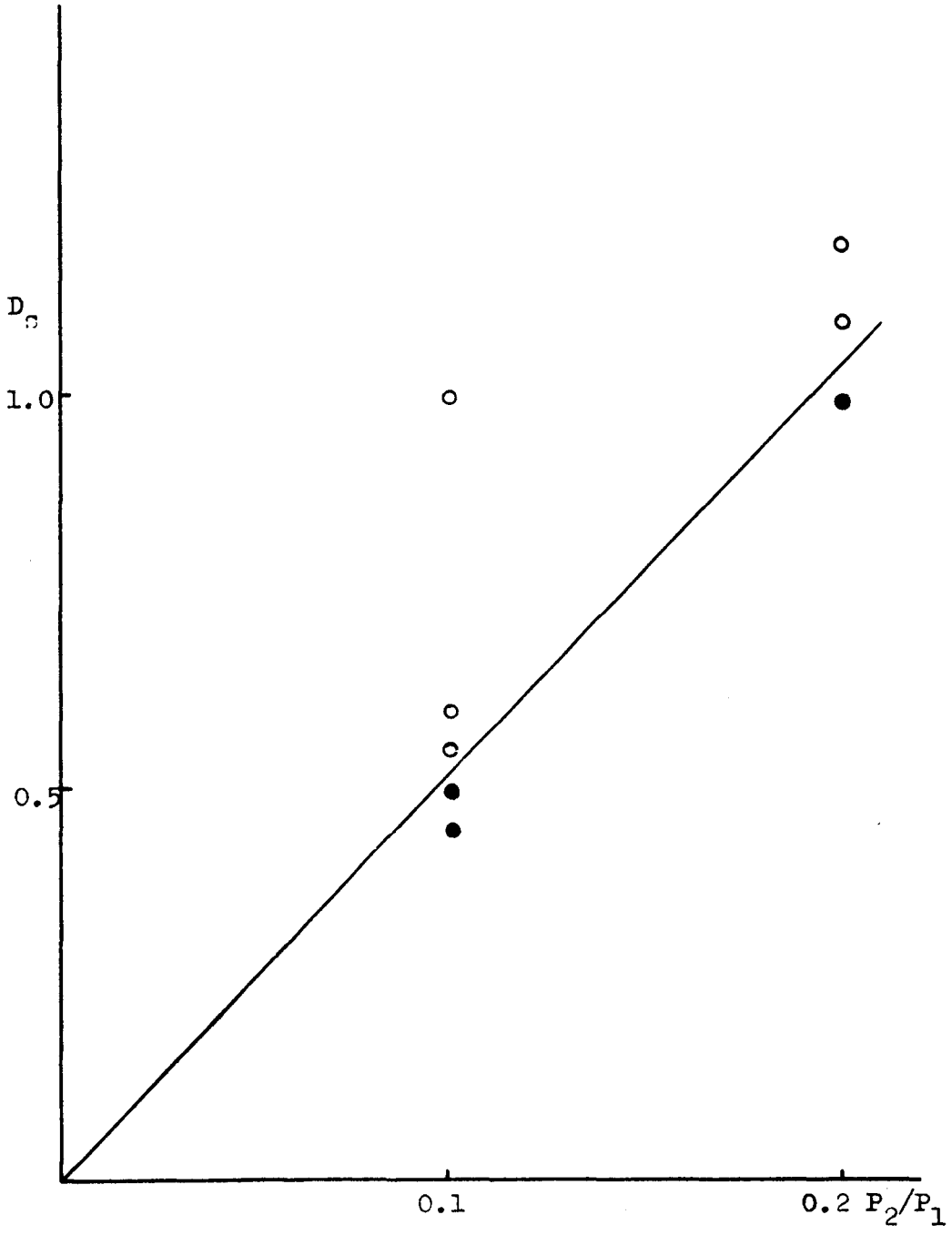

Figure 26. Quench limit obtained in computer experiments. The open symbols represent experiments in which the propellant quenched. The solid symbols represent experiments in which the propellant continued to burn. $n = 1.2$, $E = 5.56$, $\Delta h_w = 0$.

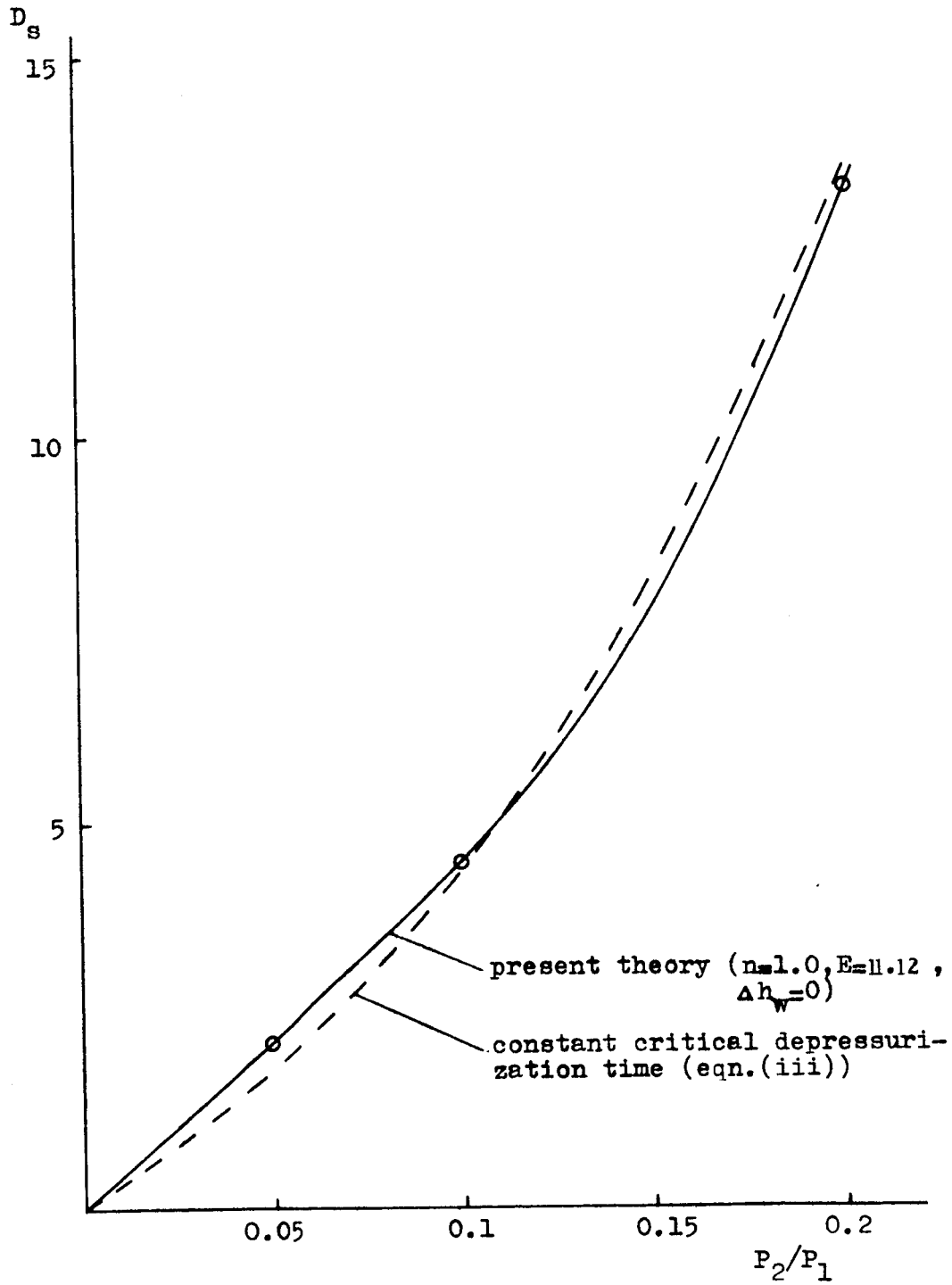

Figure 27. Comparison of the results of the present work with the expected results of a model which ascribes quench-limits to a constant critical depressurization time.